DISTRIBUTION AND MAPPING OF HIGH-MAGNESIUM CALCITE VS. ARAGONITE IN STROMATOLITES OF STORR'S LAKE, SAN SALVADOR, BAHAMAS

Senior Thesis

Submitted in partial fulfillment of the requirements for the

Bachelor of Science Degree

At The Ohio State University

By

Qingting Wu

The Ohio State University

2018

Approved by

Elizabeth M. Griffith

Elizabeth M. Griffith, Advisor

School of Earth Sciences

TABLE OF CONTENTS

ABSTRACT

Some well-developed microbial mats have calcified structures called microbialites in Storr's Lake, a hypersaline lake on the east coast of San Salvador Island, Bahamas. Many of theses microbialites are laminated, and therefore classified as stromatolites. This study focuses on a small stromatolitic knob collected from the bottom of Storr's Lake, whose mineralogy is dominated by aragonite and high-Mg calcite. These two minerals appear to dominate different layers that are classified by the depth below the top surface of samples. This study concentrates on mapping and finding the distribution of these two minerals. Titan-Yellow staining colorfully distinguished mineralogical spatial distribution in stromatolites, while a higher resolution of aragonite and high-Mg calcite distribution was accomplished by using a Scanning Electron Microscope. The stromatolitic intervals include oriented, wavy to parallel carbonate and organic-rich laminae from Titan-Yellow stainning results, as well as 1 mm diameter spherules with laminae of aragonite. Botryoidal aragonite is either discontinuous (distinct botryoids) or forms more continuous laminae (coalesced botryoids). This project can be used to inform future studies of fine-grained stromatolites in the fossil record, and discussion about controls and formation procedure on the mineralogical compositions.

ACKNOWLEDGEMENTS

I would like to thank all of those who supported this research for my senior thesis. American Chemical Society Petroleum Research Fund 54853-ND2 and The Friends of Orton Hall fund (FOH), as well as The School of Earth Sciences Field Experiences Fund supported me financially. I certainly appreciate their generosity, without them, this research will not proceed smoothly.

I would like to present my sincere appreciate to my thesis advisor, Dr. Elizabeth Griffith. Even though she is new to Ohio State University and barely knew me before, Dr. Griffith provided me with numerous trusts and assistance. She is not only the supplier of experimental samples but also the provider of ideas and inspirations of this thesis. She is the captain that makes sure everything is on track. Thanks to her, I have an opportunity to work in the field of geochemistry.

I would also like to thank Dr. Julia Sheets and Dr. Sue Welch for helping in the SEMCAL. Dr. Welch gave me lots of good suggestions on how to deal with the thin sections and how to stain them. Dr. Sheets has trained me to work on the Leica DMS1000 microscope. Both of them provided me with plenty of help on SEM (Scanning Electron Microscope) observations, which is time-consuming. Thanks again for their contributions to my research.

Furthermore, I would like to thank Dr. Griffith's previous graduate student, Mr. Zijian Li, who investigated stromatolites in Storr's Lake and offered a comprehensive research based on it. Without his work, I would not have the chance to look at these samples and gain some inspirations from his research. Zijian Li's previous work laid the foundation largely for my research.

Finally, I would like to express my gratitude to my families. Without their support and encouragement, I will not be able to go this far. They are always the spiritual pillars when I am facing hardship.

LIST OF FIGURES

INTRODUCTION

Stromatolites are a type of microbialite (benthic microbial deposits; Burne & Moore, 1987) with characteristic mesoscopic lamination resulting from complex interactions between extrinsic and intrinsic factors (Reid *et al*., 2003; Riding, 2011; Bosak *et al*., 2013). The formation of these laminated microbialites involves two main processes: (1) the trapping and binding of sediment and (2) the precipitation of carbonate minerals (e.g., Monty, 1977; Riding 2000, 2011). Both of these processes are controlled by the properties of the depositional environment, for example, the amount and type of sediment, and the carbonate minerals' saturation state (e.g., saturated, under-saturated or over-saturated).

In the scientific community, stromatolites receive attention because they are believed to be among the oldest traces of life in the rock record (Hofman *et al.*, 1999; Allwood *et al.*, 2006, 2007). On the early Earth, before the appearance of plants, animals and other eukaryotes, stromatolites could have dominated the global carbon cycle or affected the state of Earth's climate and atmosphere. Thus, understanding ancient stromatolites is critical to understanding Earth's history.

Although X-ray diffraction (XRD) studies confirmed the presence of both Mg-calcite and aragonite in the plateau-mushroom and pinnacle mound microbialites used in this study, only Mg-calcite was identified in other microbial morphotypes from the study site (Paul et al., 2016). A precise and direct distribution of Mg-calcite and aragonite in stromatolites used in this study is not provided. Staining thin sections with Titan yellow and fixing them with sodium hydroxide solution should achieve accurate spatial recognition of Mg-rich calcite in thin sections of these microbialites. In this way, a better understand of the formation of ancient fossil stromatolites, especially the Mg isotopic composition can be developed (Choquette & Trusell, 1978; Li, 2017). Furthermore, SEM (scanning electron microscopy) can provide detailed high-resolution images of the sample, particularly showing the boundary of Mg-calcite and aragonite, by rastering a focused electron beam across the surface and detecting secondary or backscattered electron signal.

Previous work by Zijian Li (2017) indicated that Mg isotopic compositions of microbialite sublayers could be controlled by the percentage of aragonite versus Mg-calcite, suggesting that the transformation from aragonite to calcite (or vice versa) is important and necessary to study in order to have a comprehensive understanding of strmatolites' formation process of Storr's Lake (study site).

GEOLOGIC SETTING

Storr's Lake is a hypersaline lake on the northeastern, windward coast of San Salvador Island, which is located on a small, isolated bank at the eastern edge of Bahamas (Curran, 1997).

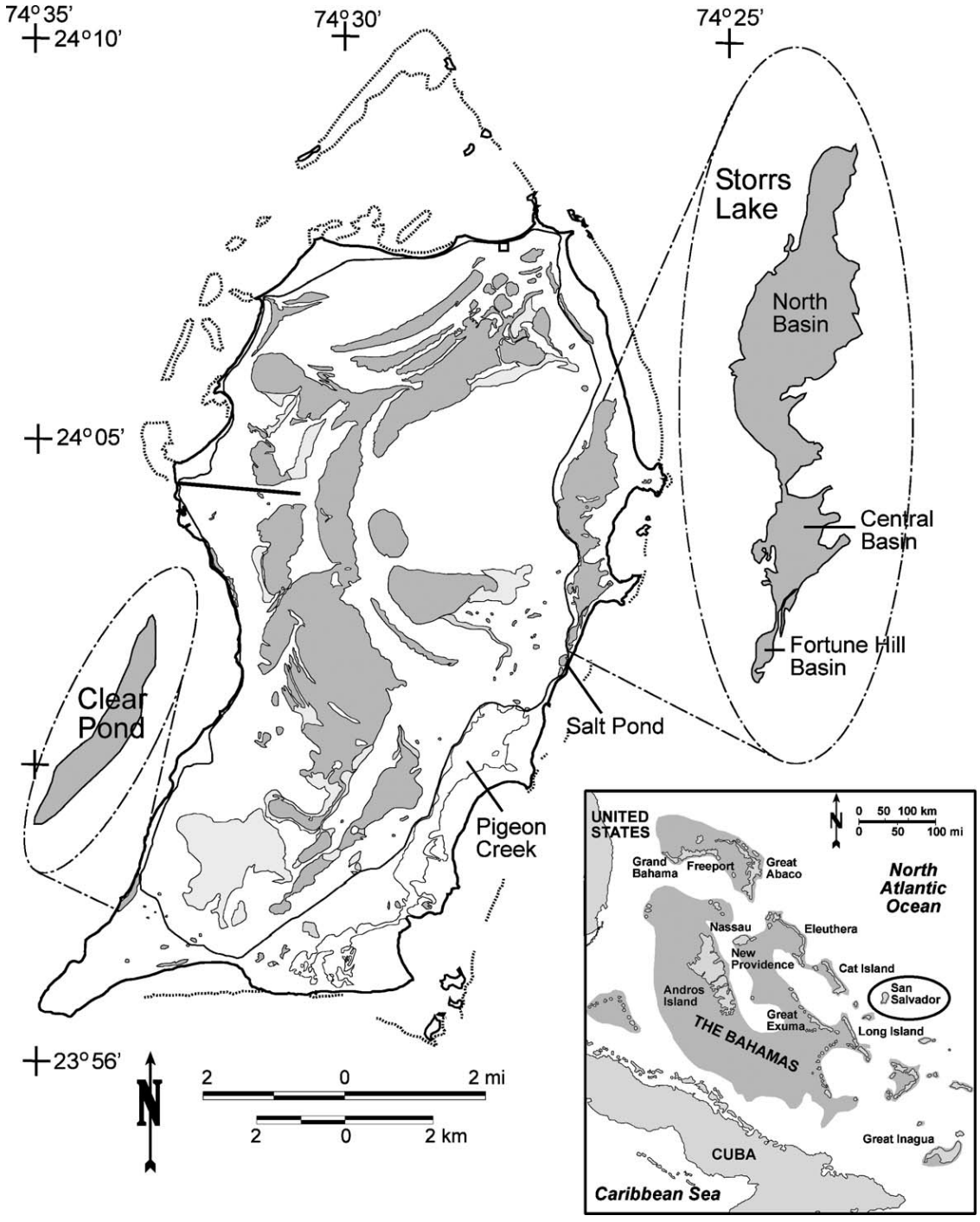

Figure 1. Location map of Storr's Lake within San Salvador Island, The Bahamas (figure from Park, 2012)

Storr's Lake is composed of a larger, deeper northern section ("North Basin") and a smaller, shallower southern section ("Central Basin"), which is separated by a small zone called "the narrows" (Zabielski, 1991; Figure 1). Storr's Lake is a shallow lake that only reaches a maximum depth of two meters, and the water levels fluctuate throughout the year (Fowler, 2011).

The northern section of Storr's Lake has been the focus by more scientists than the southern section. Extensive carbonate sediments have developed here for the past 3000 years (Hattin, 1982), and various microbialite structures have been classified by depth (Mann & Nelson, 1989). Based on previous invastigation, the northern section of Storr's Lake can be divided into five zones; from shallow to deep are soft algae mounds, microbial mat (coarse sediment), bulbous crusts, mushroom-shaped heads and club-shaped heads (Neumann *et al*., 1989; Mann & Nelson, 1989; Paull *et al*., 1992).

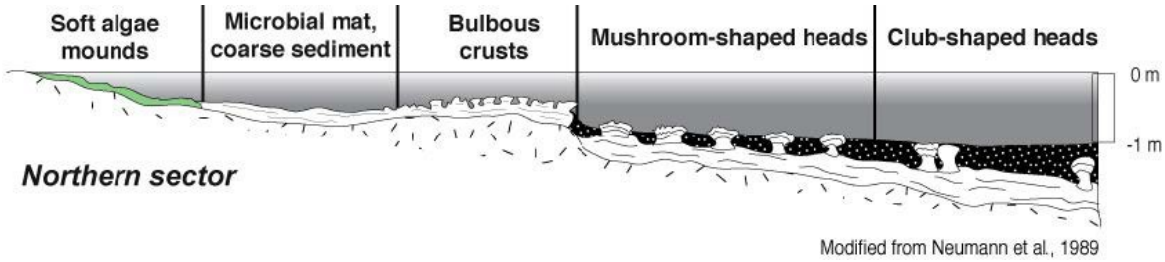

Figure 2. Storr's Lake Northern Sector Zones (figure from Fowler, 2011)

The southern section is smaller and shallower than the northern section, and the average salinity and temperature of the lake are ~60 ‰ and ~26°C, respectively, with the pH ranging from ~8.1 to ~8.6 (Fowler, 2011). In comparison to northern sections, the southern sections exhibit higher ionic concentrations because southern sections of the lake are shallower than the northern sections and would be more strongly influenced by evaporation (Glumac & Savarese, 2016).

For this study, the sampling location was in the southwestern section, labeled as WS-1 (Figure 3), stromatolitic knobs were collected manually from the bottom of Storr's Lake (Figure 4). Zijian Li (2017) made thin sections at The University of Texas at Arlington.

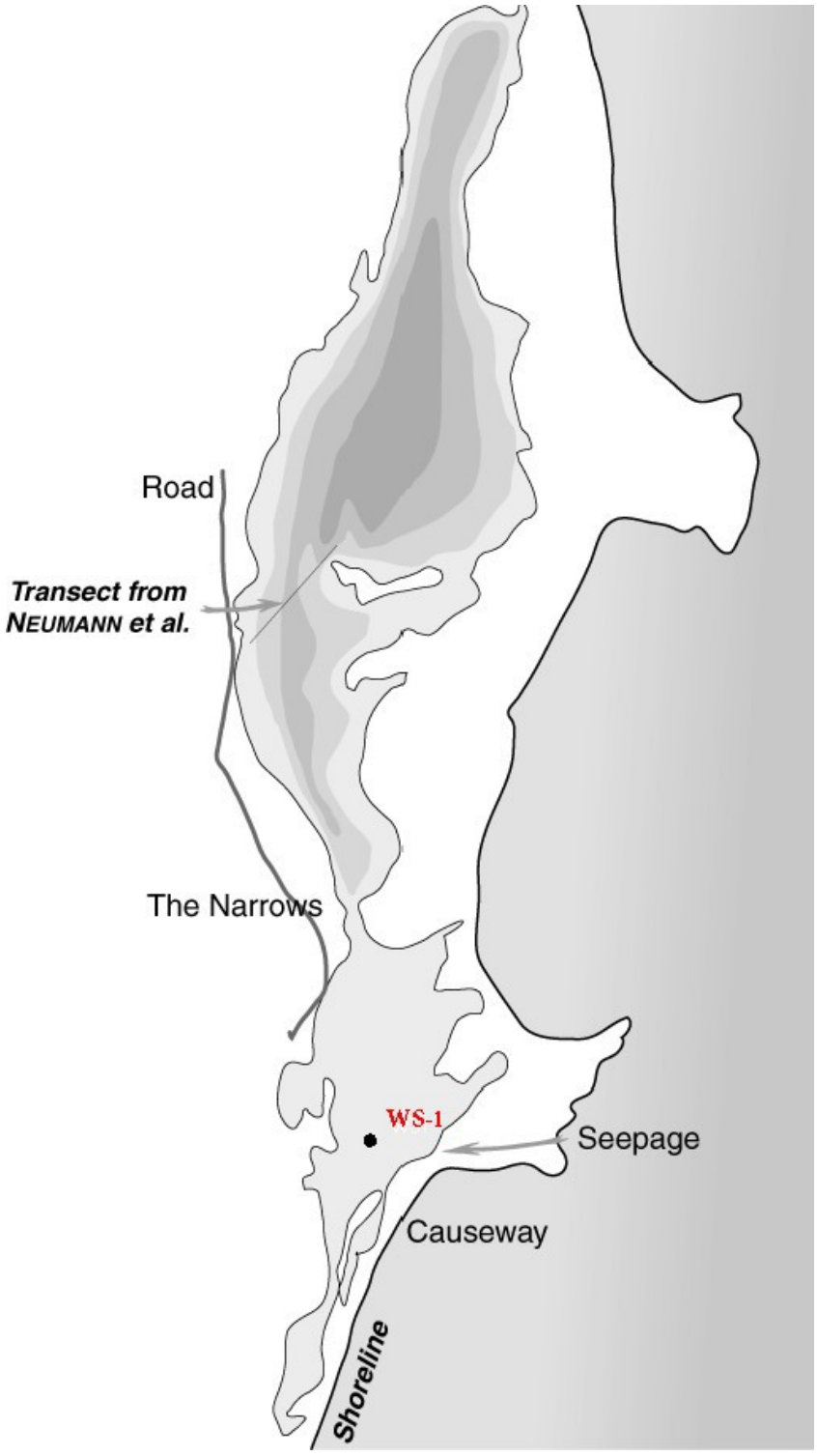

Figure 3. Sampling Location in Storr's Lake (figure from Dupraz, 1999)

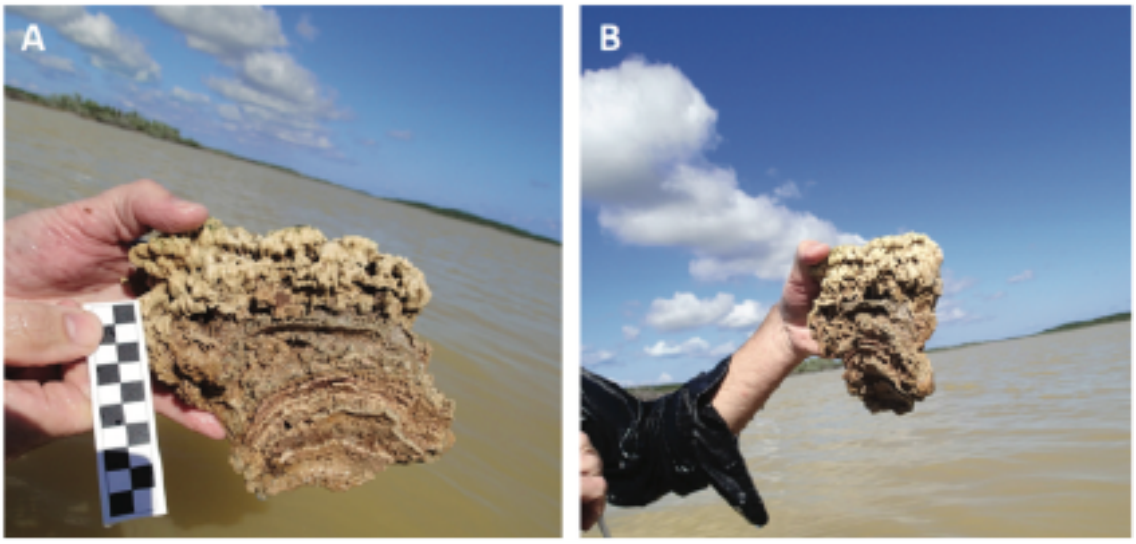

Figure 4. (A) Front view, (B) Side view of mound sample WS-1 (Li, 2017)

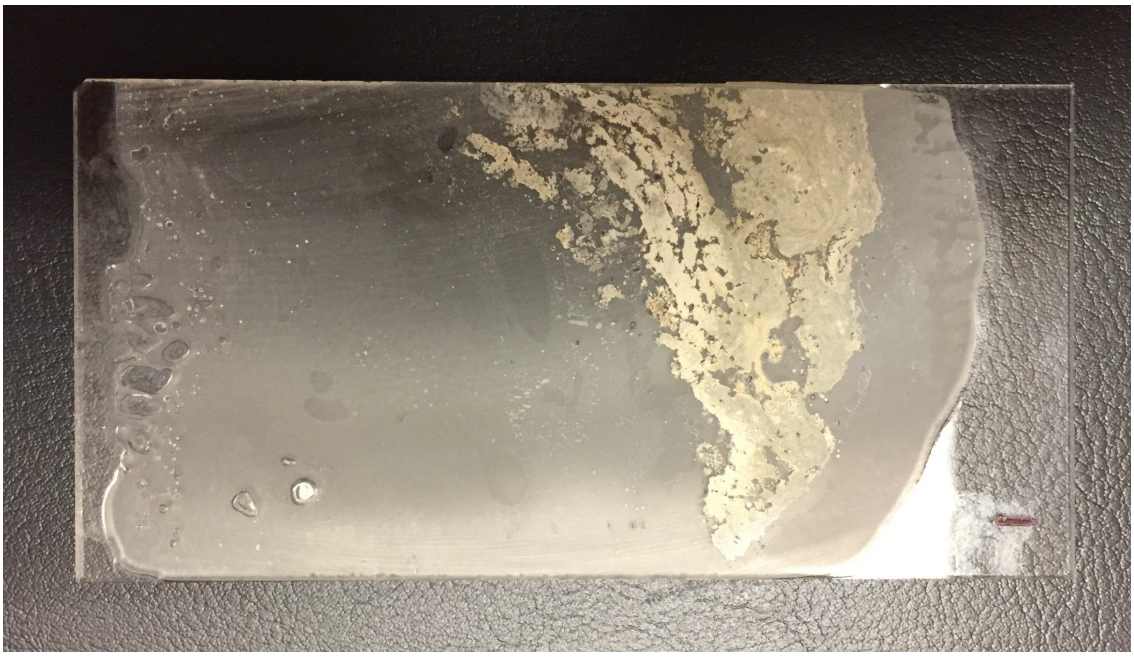

Figure 5. Thin section of mound sample's transverse section from the base of WS-1

Methods

Titan-Yellow Stain

Staining of the thin section in the laboratory was done at The Ohio State University. The procedure followed the methodology of Choquette & Trusell (1978) which includes two main steps, one is staining and the other is fixing. To start the work, two solutions were prepared ahead, one for stain and the other for fixer, as follows: STAIN: 0.5060 gram Titan-Yellow (powder, C.I. 19540)

4.0246 gram Sodium Hydroxide (NaOH)

2.0443 gram EDTA ($C_{10}H_{16}N_2O_8$)

0.5000 liter distilled water

FIXER: 100.0053 gram NaOH pellets

0.5000 liter distilled water

The two solutions are stored at room temperature and out of direct sunlight using foil cover. Both of the solutions were stored in polyethylene bottles in case of corrosion with glass. Under these conditions, thin sections were treated as follows:

1. Etch uncovered thin section about 15 seconds with 25% concentration acetic acid solution on clean watch glass.
2. Transfer thin section and watch glass to airflow workstation and air-dry thin section for 20 minutes.
3. Immerse thin section in stain solution for 20 minutes on clean watch glass.
4. Transfer thin section and watch glass to airflow workstation and air-dry thin section for 20 minutes.
5. Immerse thin section in fixer solution for 30 seconds on clean watch glass.
6. Transfer thin section and watch glass to airflow workstation and air-dry thin section for 20 minutes.

Saturations of the stain color increase generally toward more vivid reds with increasing Mg content, and finer crystalline Mg-calcite constituent (Choquette & Trusell, 1978).

Leica Microscopy

Microscope works accomplished in the SEMCAL (Subsurface Energy Material Characterization and Analysis Laboratory), Ohio State. The entire process took two days in total, one day for imaging unstained thin section (area size: 7.5cm * 4.0cm) and the other day is for stained thin section. A Leica DMS1000 microscope was used. The Leica DMS1000 digital microscope system is highly versatile tool for viewing microscopic specimens and capturing still images. With this microscope, tiniest details of thin section were captured as 34 high-quality, full color still images. Scales include 10mm, 5mm, 2mm and 1mm. Magnification of the images range from 4x to 20x. Because Leica microscope is for locating the distribution and figuring the arrangement of calcite and aragonite, not for internal crystalline structures of two minerals, therefore, high magnification observation is not needed.

Scanning Electron Microscopy

The Scanning Electron Microscope (SEM) work completed by Dr. Julia Sheet and Dr. Sue Welch in the SEMCAL, Ohio State. SEM was used to reveal information about sample's chemical composition, including elemental maps and discrimination of phases based on mean atomic number. SEM was also used to show sample's crystalline structure and orientation of materials making up the sample.

SEM uses a focused beam of high-energy electrons that is dissipated as a variety of signals produced by electron-sample interactions, because accelerated electrons can pass through sample without interaction, undergo elastic scattering and can be inelastically scattered. Elastic and inelastic scattering result in a number of signals, including secondary electrons (generate SEM images), backscattered electrons (illustrate composition contrast), and diffracted backscattered electrons (determine crystal structures and orientation of minerals) (Swapp, 2017).

SEM was used to discriminate between high-magnesium calcite and aragonite at high spatial scales and hence the boundary area between two minerals became our focus.

Moreover, using primarily backscattered electron images and also Energy Dispersive X-ray Analyzer (EDX) to confirm elemental composition differences. The EDX was also used to create elemental maps of the sample at one location 1.5mm * 1.5mm with the accelerating voltage 15.00 kV. Magnification of the images ranges from 110x to 2000x.

Results

Titan-Yellow Stain Result

Choquette and Trusell (1978) showed that the color of calcite stained with Titan-yellow depends on its magnesium content. High-Mg calcite takes a deeper red color, while low-Mg mineral takes a pale red color. This method is powerfully selective in its ability to discriminate Mg-calcite from other carbonate minerals (aragonite). After Titan-yellow stain, Mg-calcite shows a dark orange color; in the meantime, aragonite shows a light orange color in the sample investigated for this study.

Observations using Leica DMS1000 microscope indicate the color difference of two minerals, in association with a range of arrangement types. These types are distributed randomly in the thin section and captured as figures under different magnification, including the following:

Magnification x4 — WS1 (Figure 6) & sWS1 (Figure 7)
Magnification x8 — C (Figure 24) & sC (Figure 25)
Magnification x10 — A (Figure 8) & sA (Figure 9)
B (Figure 16) & sB (Figure 17)
Magnification x20 — D (Figure 34) & sD (Figure 35)
From A’ (Figure 10) to sA’’’ (Figure 15)
From B’ (Figure 18) to sB’’’ (Figure 23)
From C’ (Figure 26) to sC’’’’ (Figure 33)
From s1 (Figure 36) to s4 (Figure 39)

I. WS1 and sWS1 represent the entire stromatolites thin section area before (Figure 6) and after stain (Figure 7) under magnification x4. There are two major colors in WS1, one is dark tan and the other is light tan. In sWS1, light orange color dominates the thin section, indicating low-Mg mineral, while minor dark orange color represents high-Mg mineral according to Choquette and Trusell (1978). Several microscopic components make up the stromatolites. These components likely include: high-Mg calcite, aragonite, and organic matter. The stromatolitic intervals include oriented, wavy to parallel carbonate and organic-rich laminae. Spherules with laminae of low Mg carbonates are common. Botryoidal aragonite is either discontinuous (distinct botryoids) or forms more continuous laminae (coalesced botryoids).

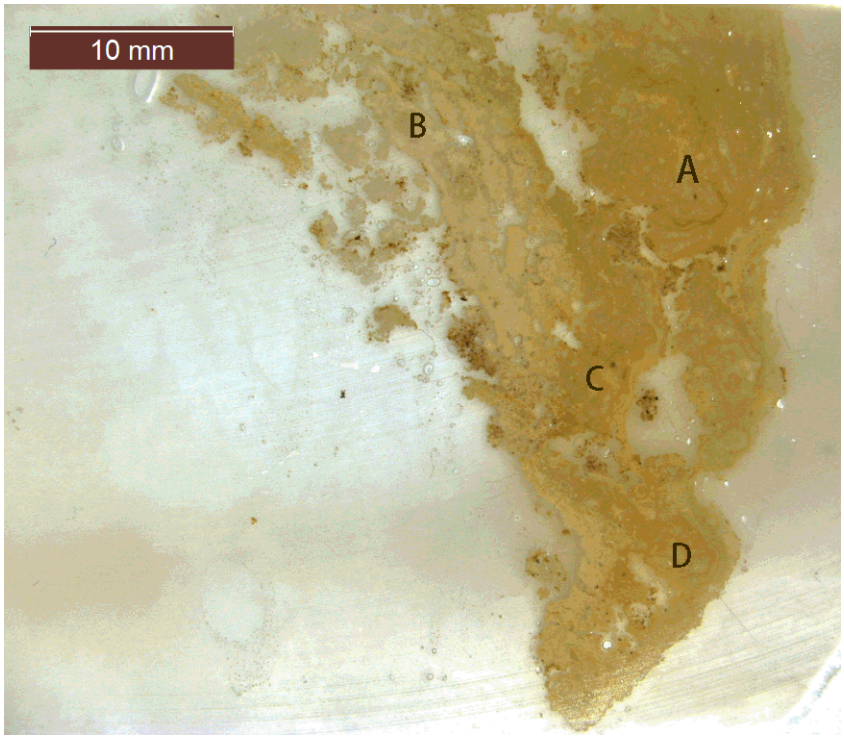

Figure 6. WS1, entire thin section before stain

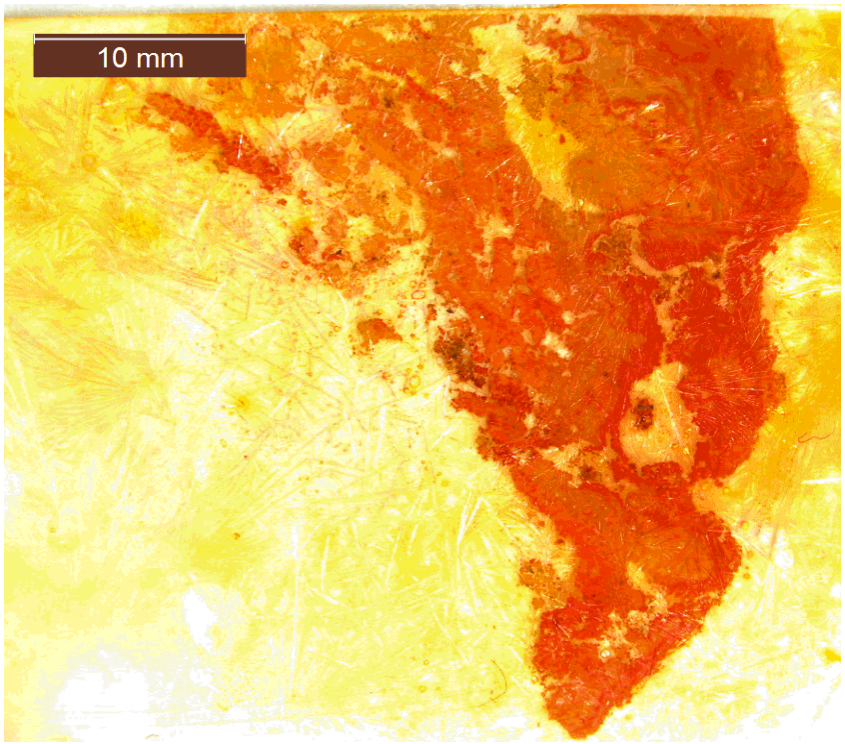

Figure 7. sWS1, entire thin section after stain

II. A (Figure 8) and sA (Figure 9) represent the upper right area of stromatolites thin section under magnification x10. Some peculiar features observed, including wavy high Mg carbonate laminae parallel to margins, meanwhile, rare low Mg carbonate spherules that are 1 mm in diameter surrounded by high Mg carbonate.

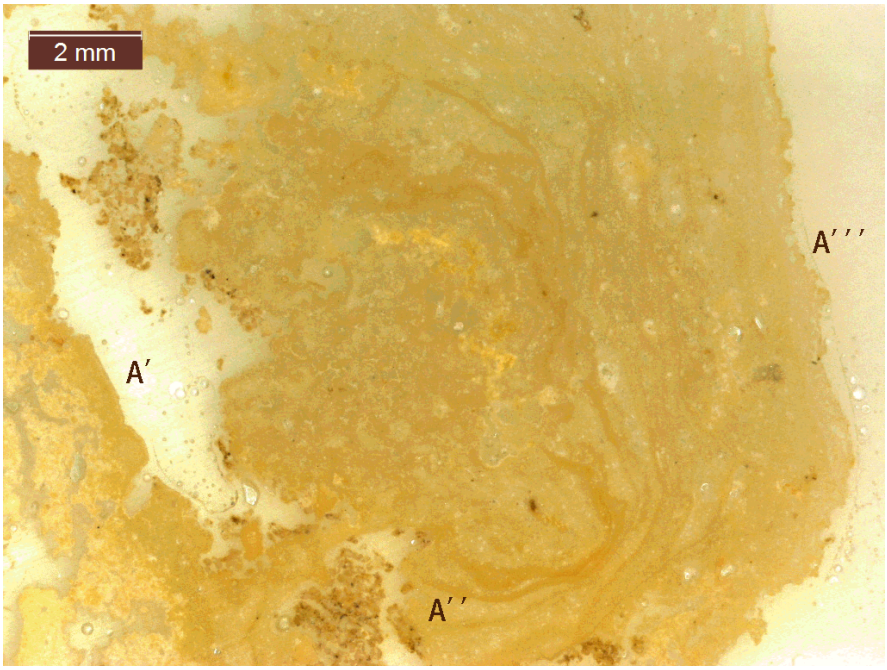

Figure 8. A, thin section of area A before stain, wavy carbonate laminae parallel to the margin

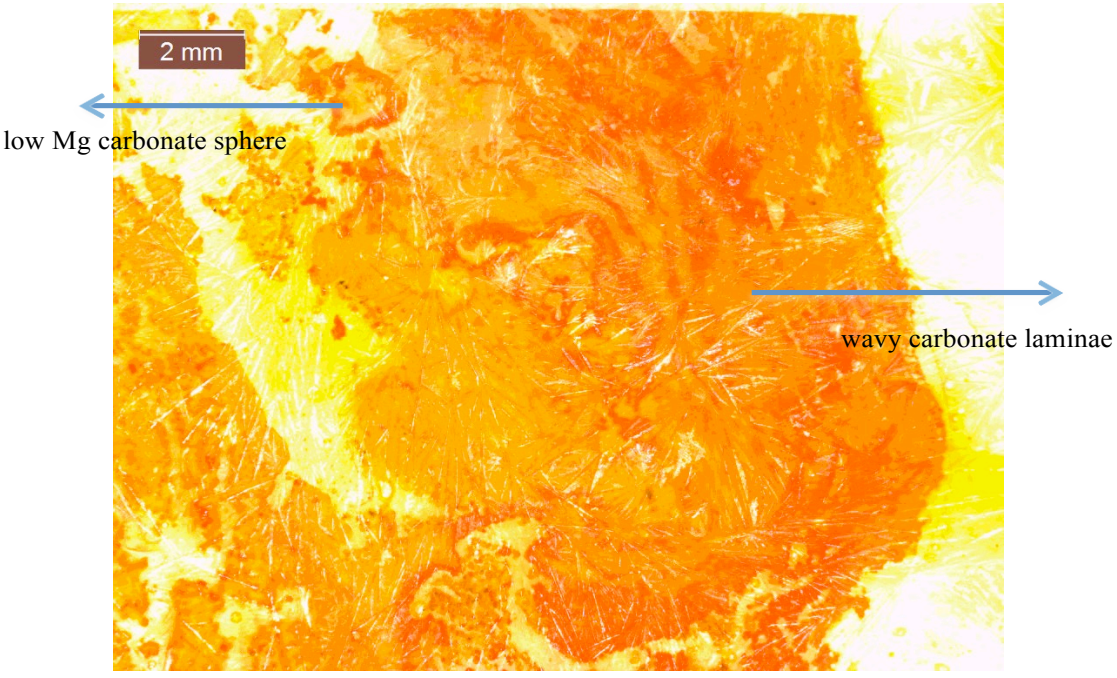

Figure 9. sA, thin section of area A after stain, low Mg carbonate sphere surrounded by high Mg carbonate

III. A’ (Figure 10) and sA’ (Figure 11) represent left sector zone of area A under magnification x20. Organic matter and fibrous high-Mg carbonate were captured.

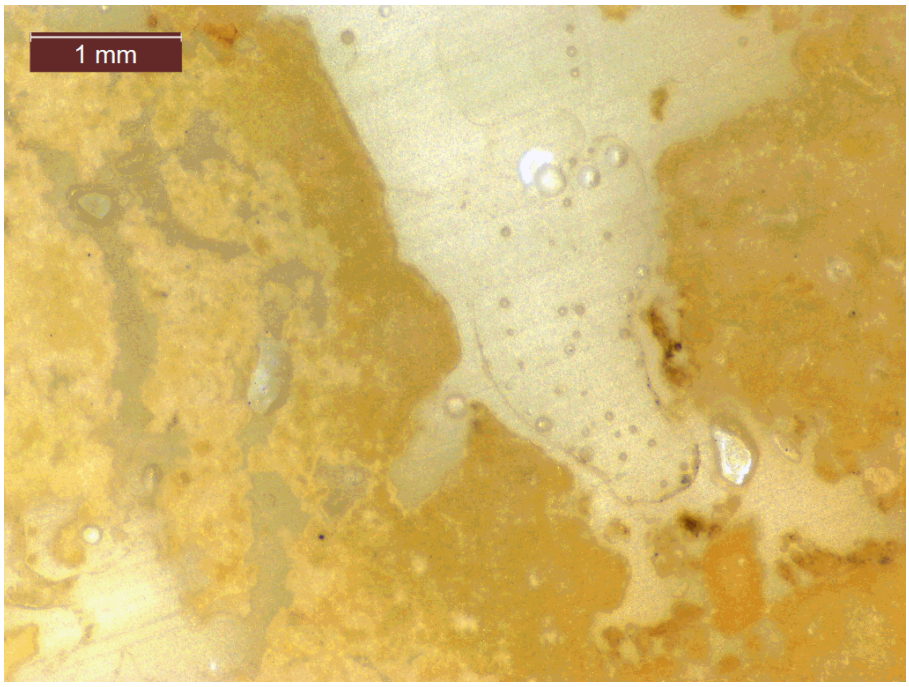

Figure 10. A’, thin section of area A’ before stain

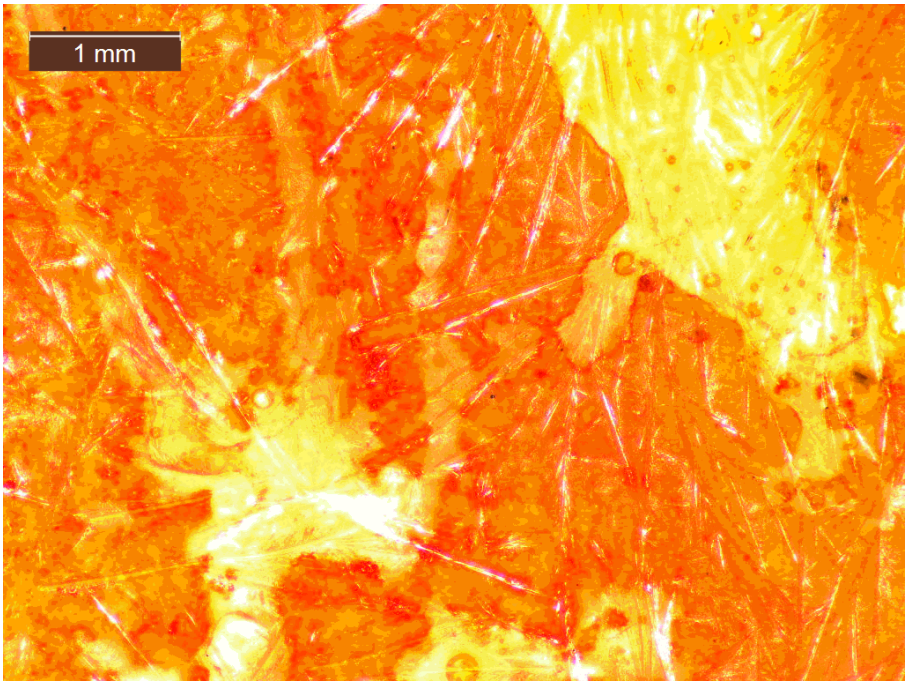

Figure 11. sA’, thin section of area A’ after stain

IV. A'' (Figure 12) and sA'' (Figure 13) represent lower sector zone of area A under magnification x20. Organic matters clot separately in the center, associated with high Mg carbonate laminae parallel to margin. Botryoidal low Mg carbonate is discontinuous towards the right of the image (distinct botryoidal).

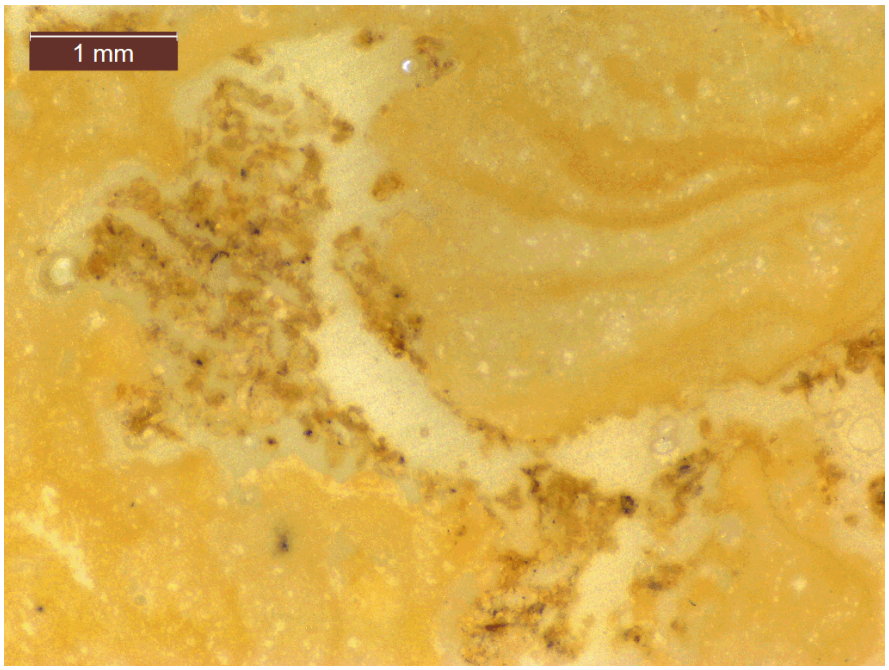

Figure 12. A'', thin section of area A'' before stain

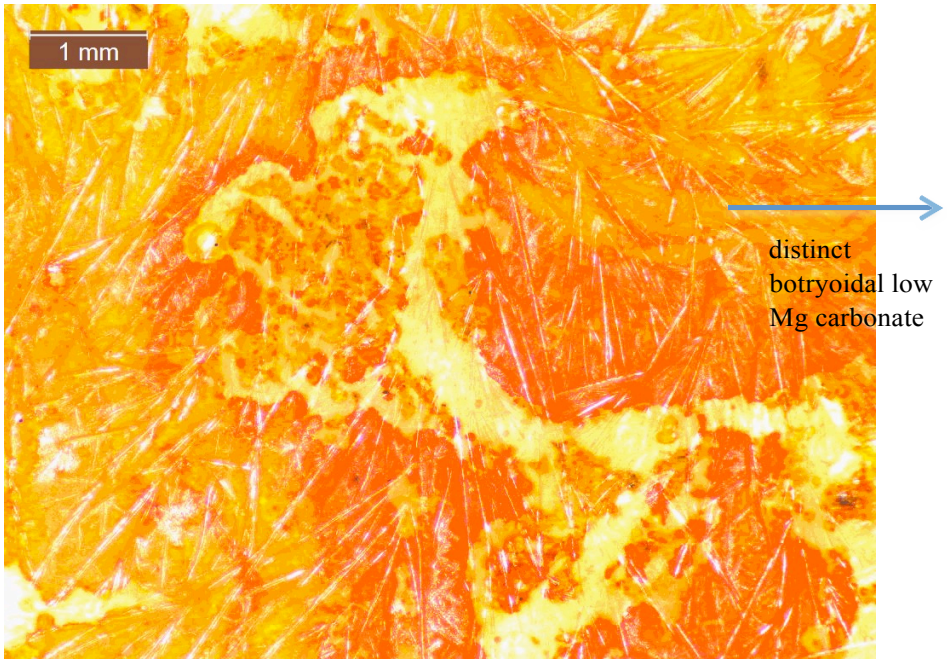

Figure 13. sA'', thin section of area A'' after stain

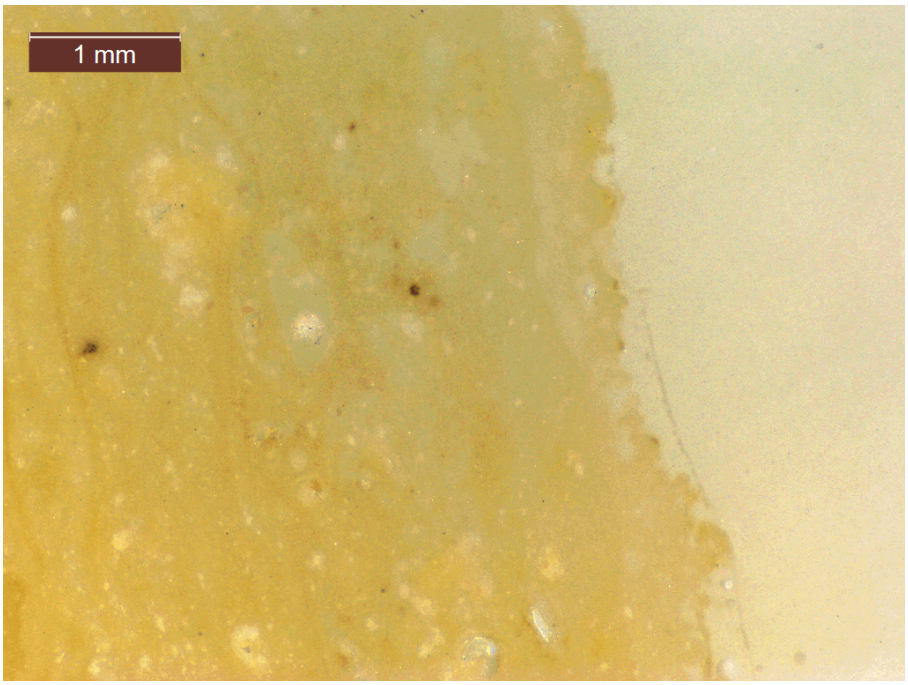

Figure 14. A’’’, thin section of area A’’’ along the margin before stain

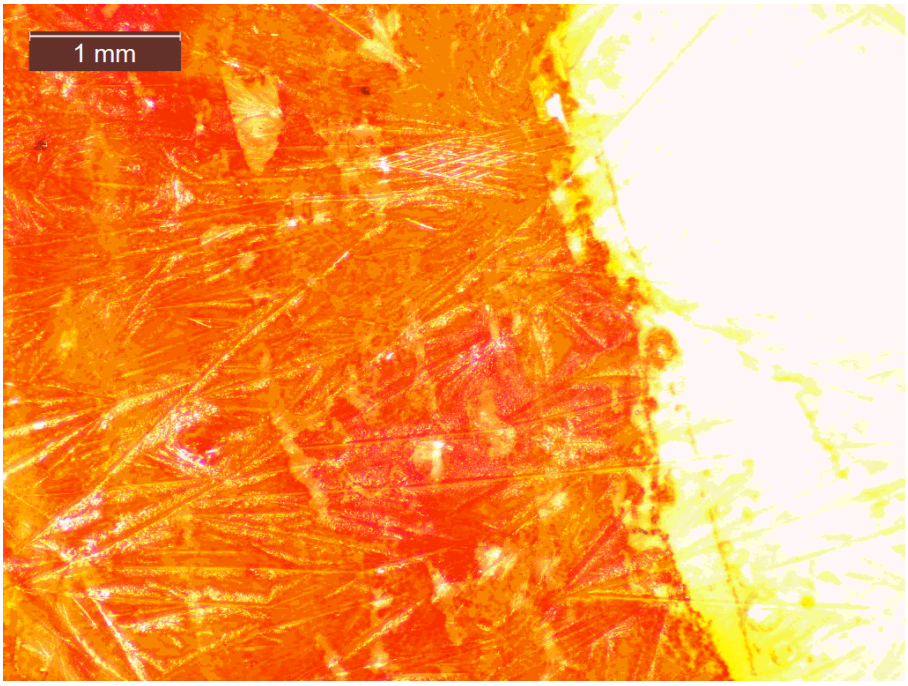

Figure 15. sA’’’, thin section of area A’’’ along the margin after stain

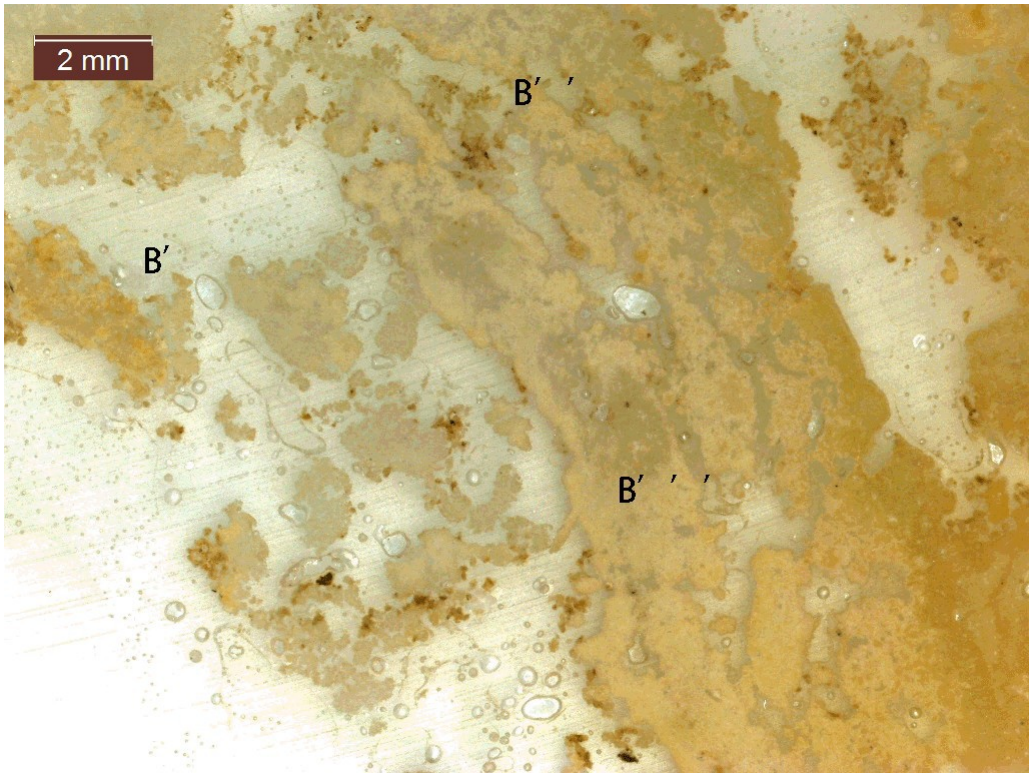

Figure 16. B, thin section of area B before stain, carbonates is sporadic with minor organic matter

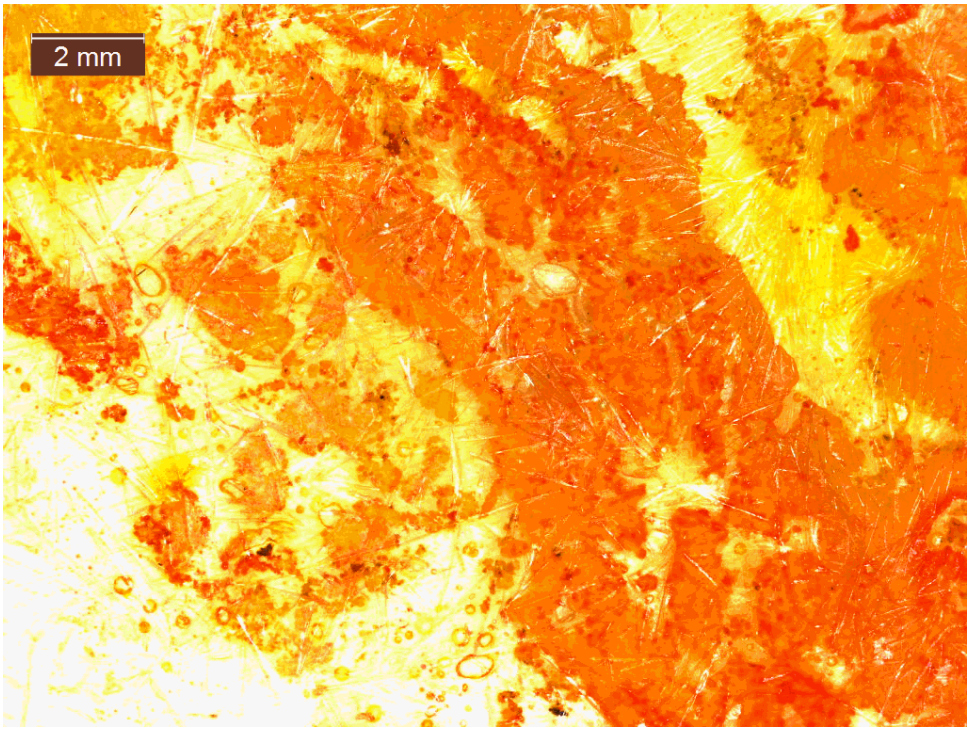

Figure 17. sB, thin section of area B after stain

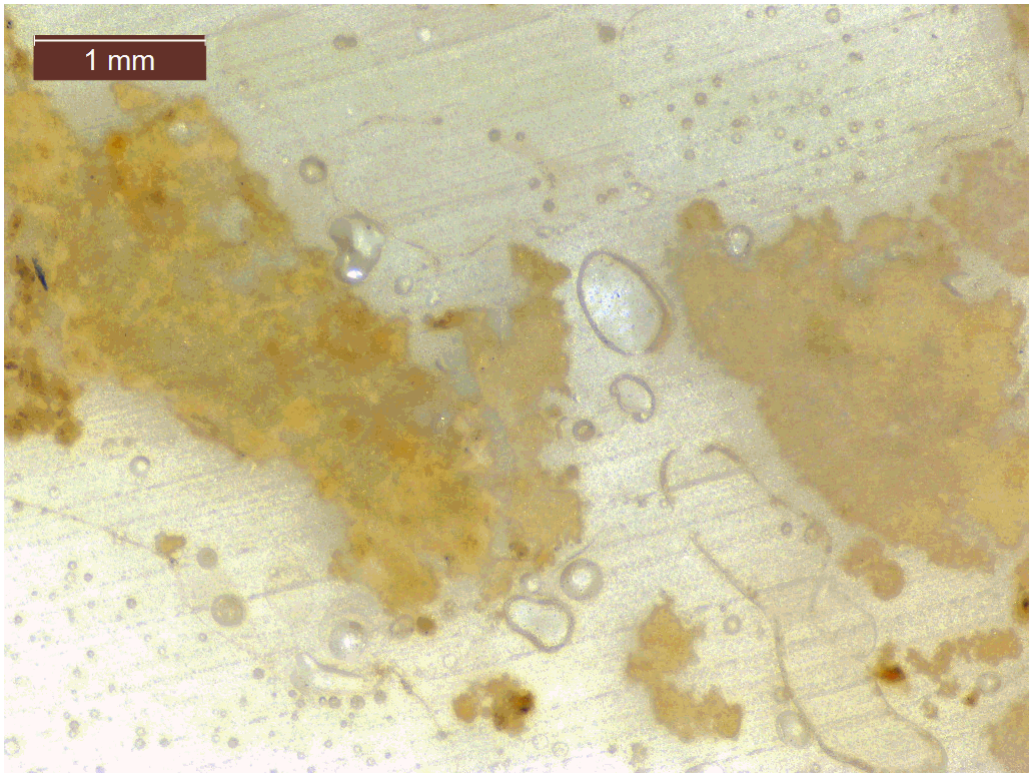

Figure 18. B', thin section of area B' before stain

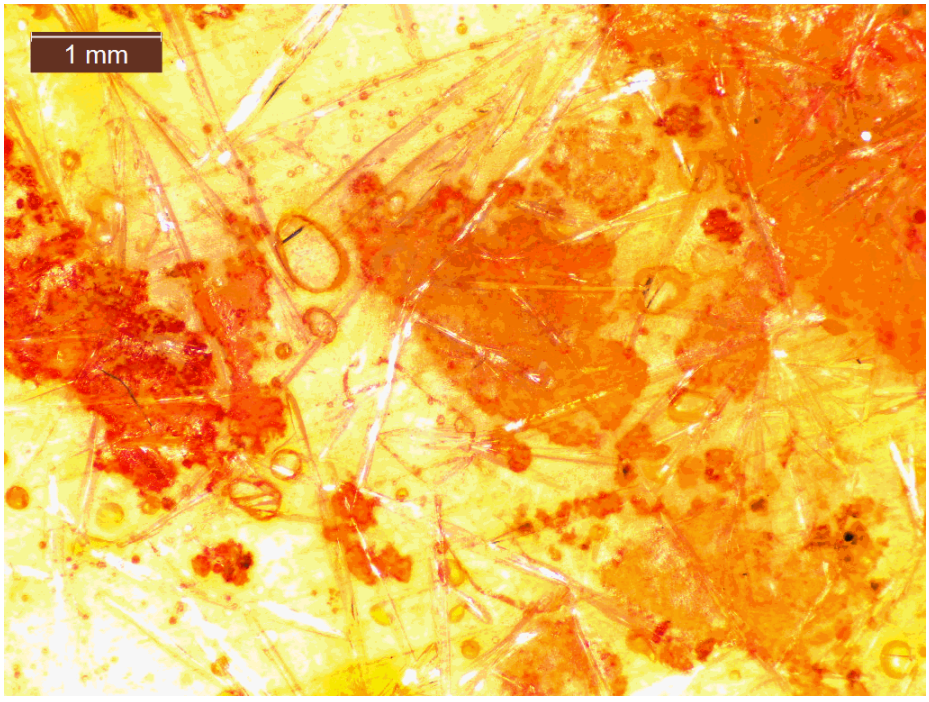

Figure 19. sB', thin section of area B' after stain

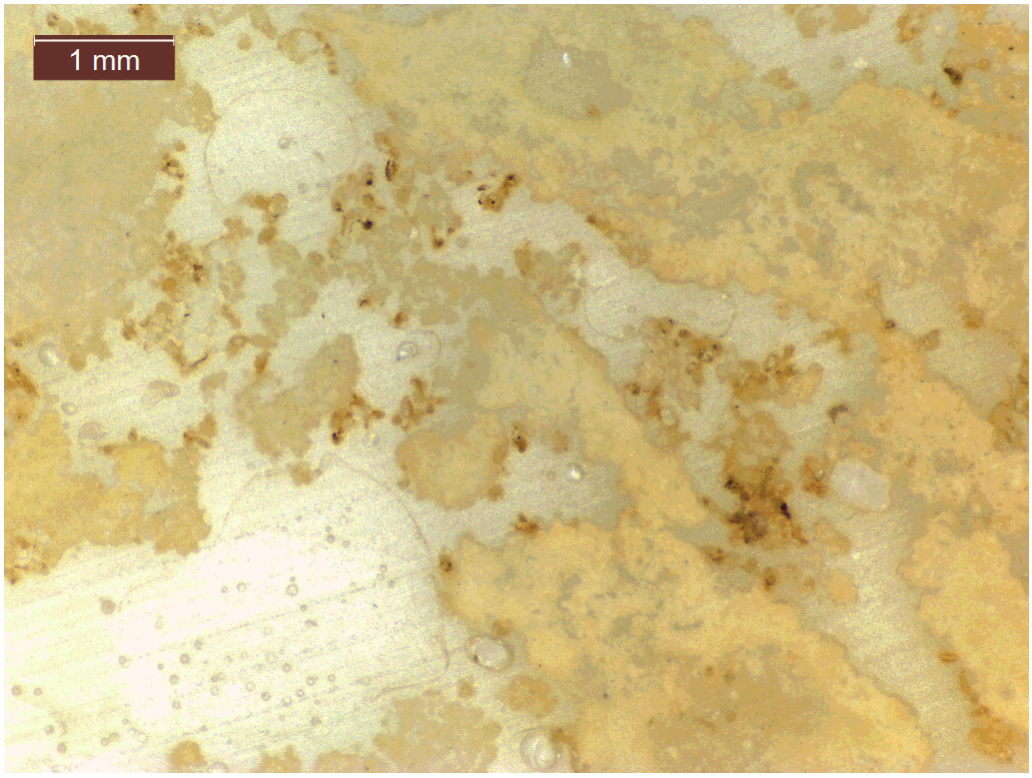

Figure 20. B’’, thin section of area B’’ before stain, carbonates distribute discontinuously

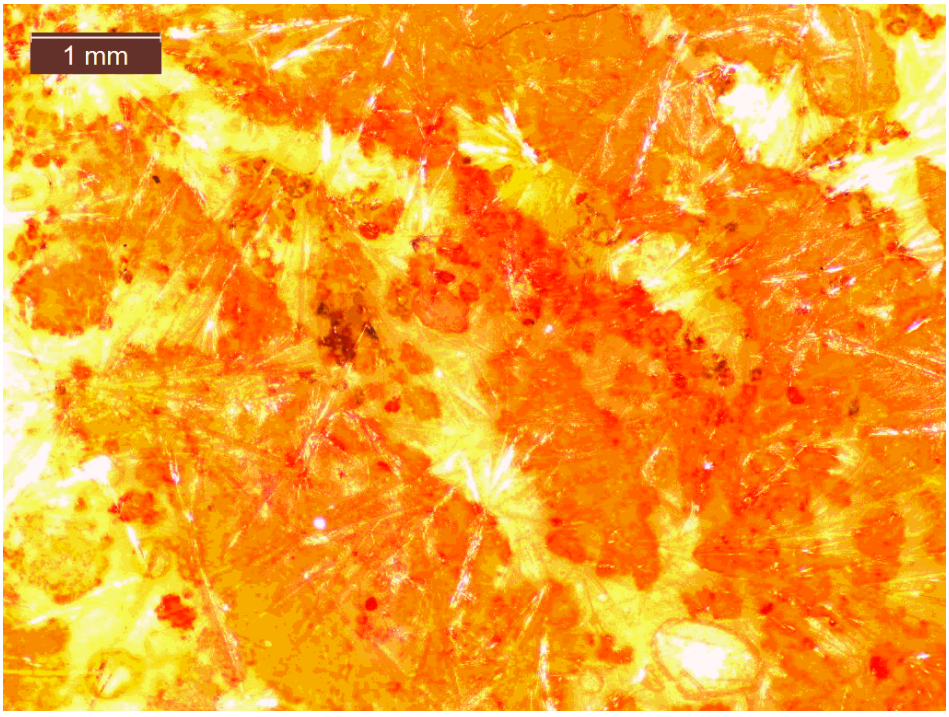

Figure 21. sB’’, thin section of area B’’ after stain

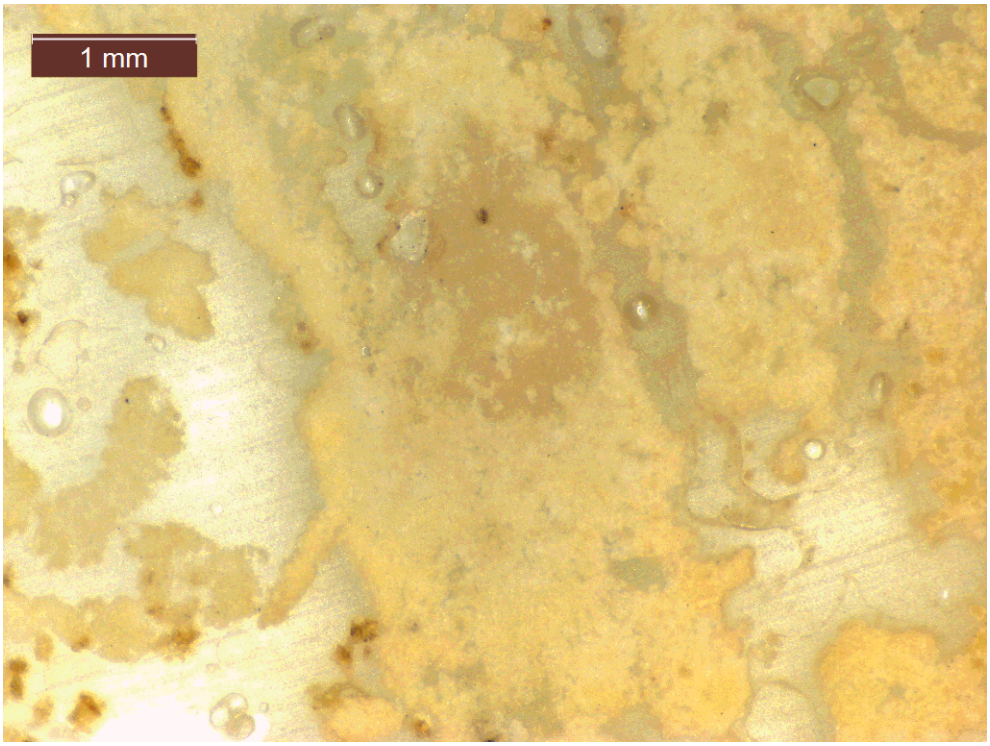

Figure 22. B’’’, thin section of area B’’’ before stain

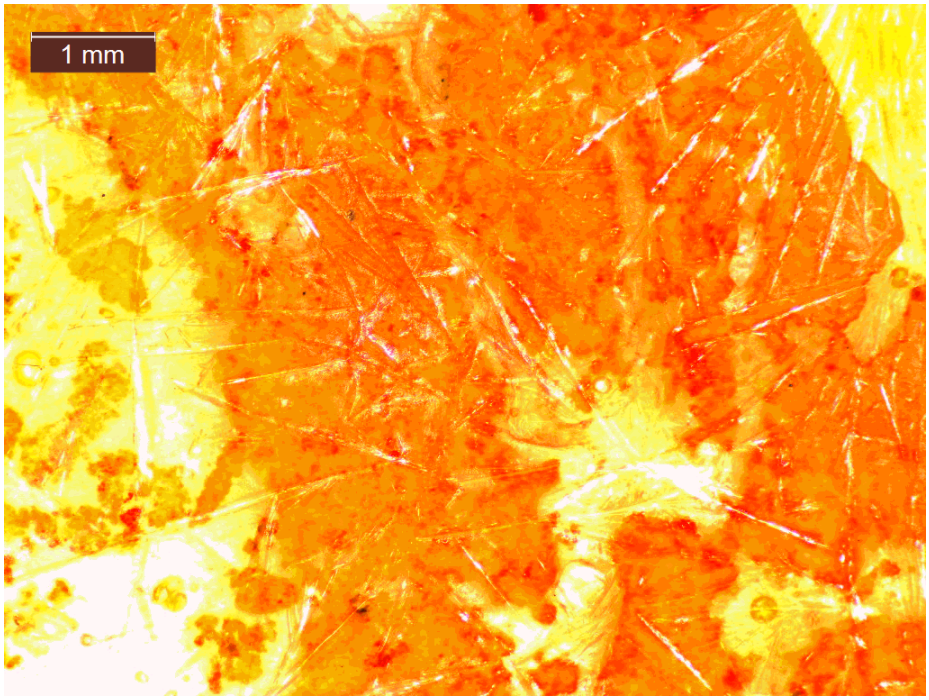

Figure 23. sB’’’, thin section of area B’’’ after stain

Figure 24. C, thin section of area C before stain

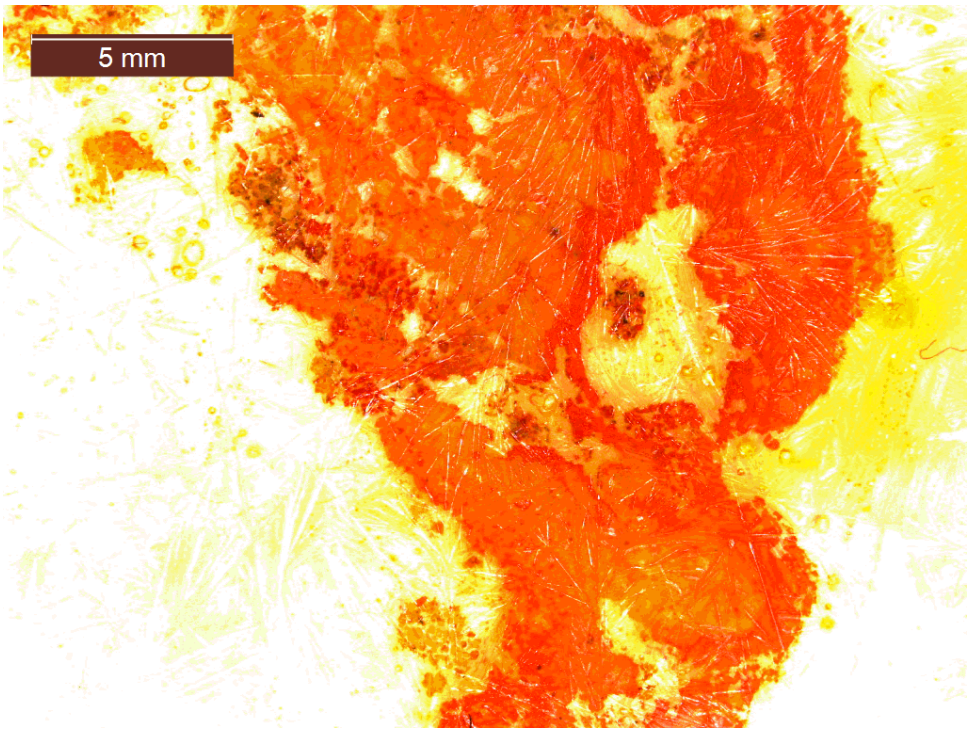

Figure 25. sC, thin section of area C after stain

Figure 26. C', organic matter clot appears in the top right corner

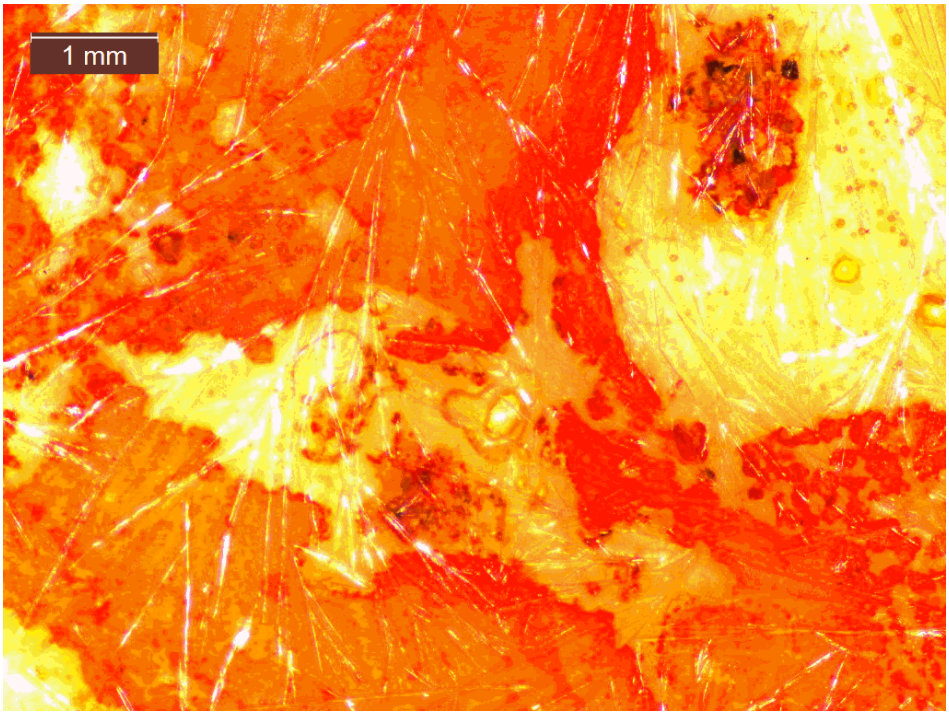

Figure 27. sC', high Mg carbonate formed along the margin

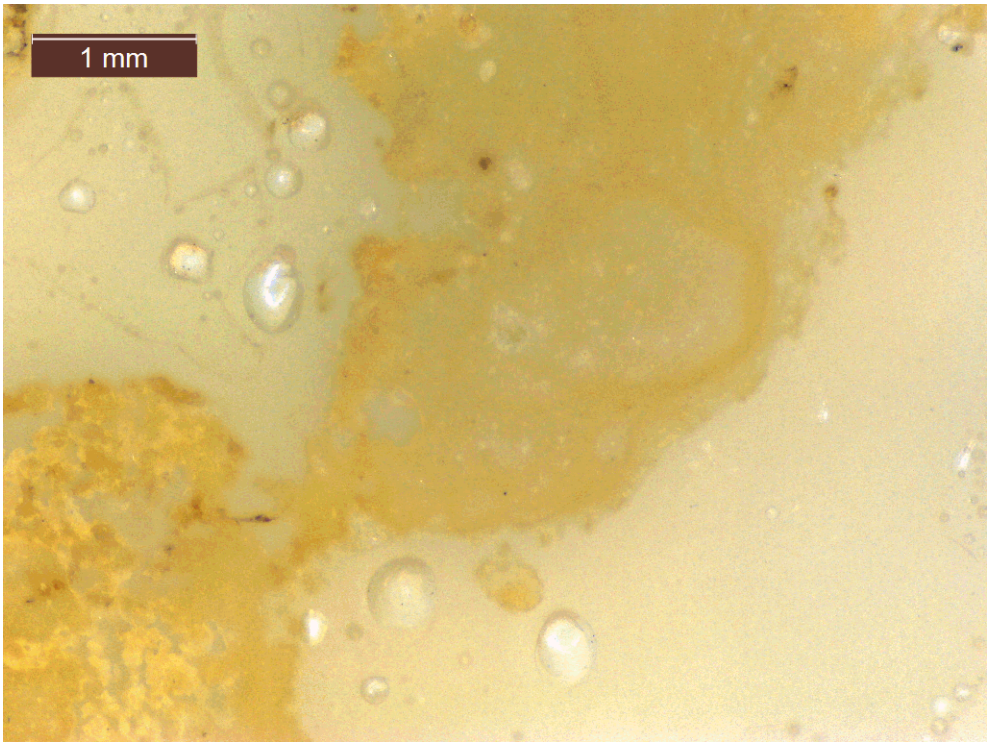

Figure 28. C’’, thin section of area C’’ before stain

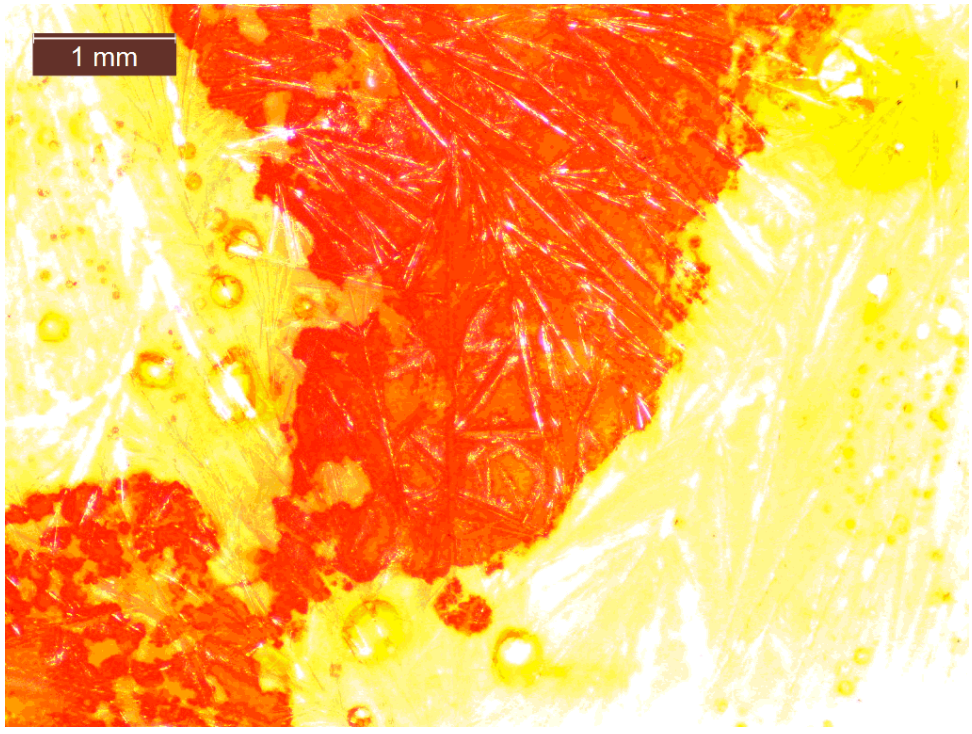

Figure 29. sC’’, thin section of area C’’ after stain

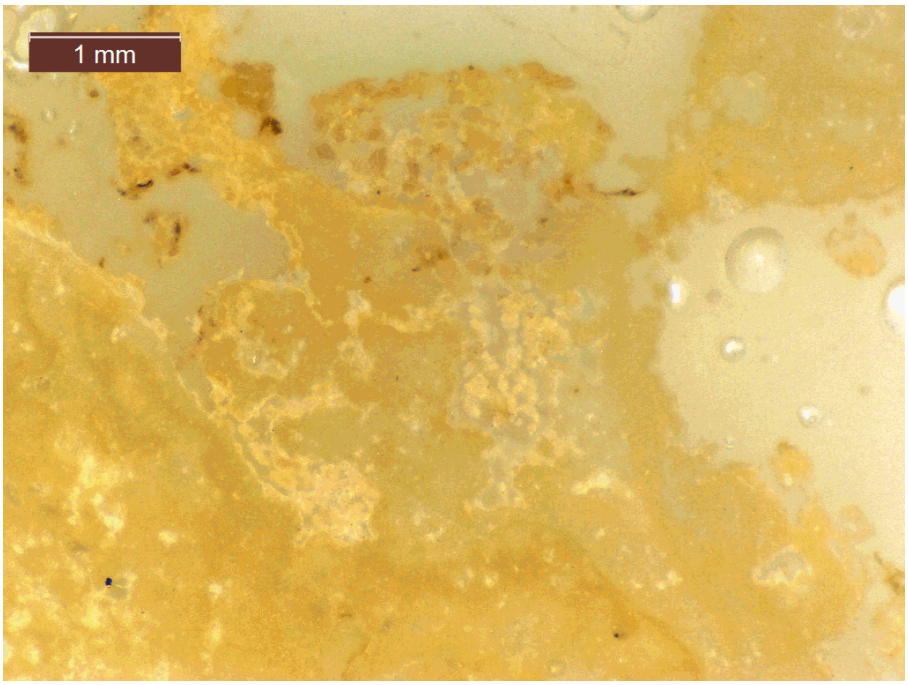

Figure 30. C’’’, thin section of area C’’’ before stain

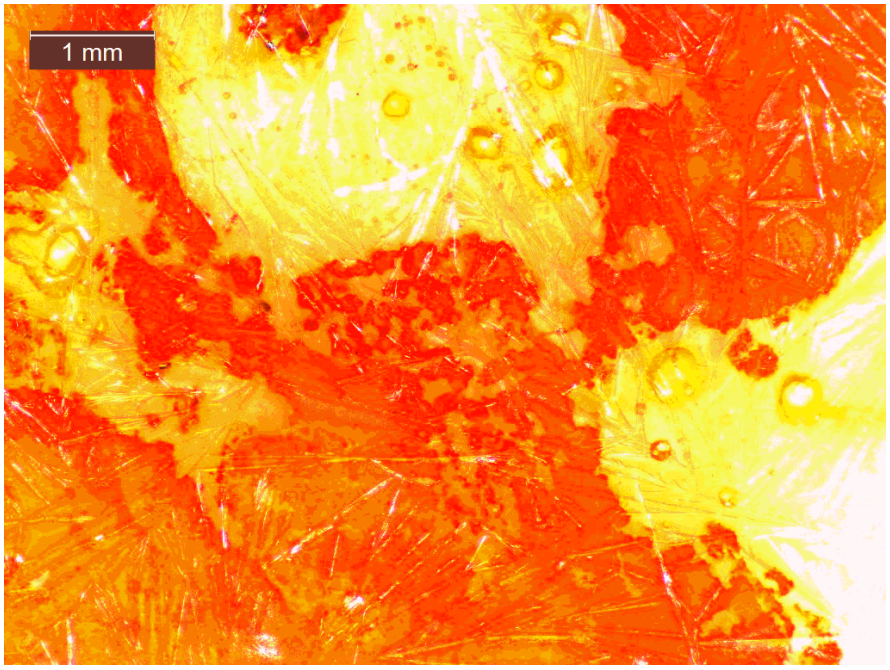

Figure 31. sC’’’, thin section of area C’’’ after stain, high Mg carbonate formed along the margin in the bottom left corner

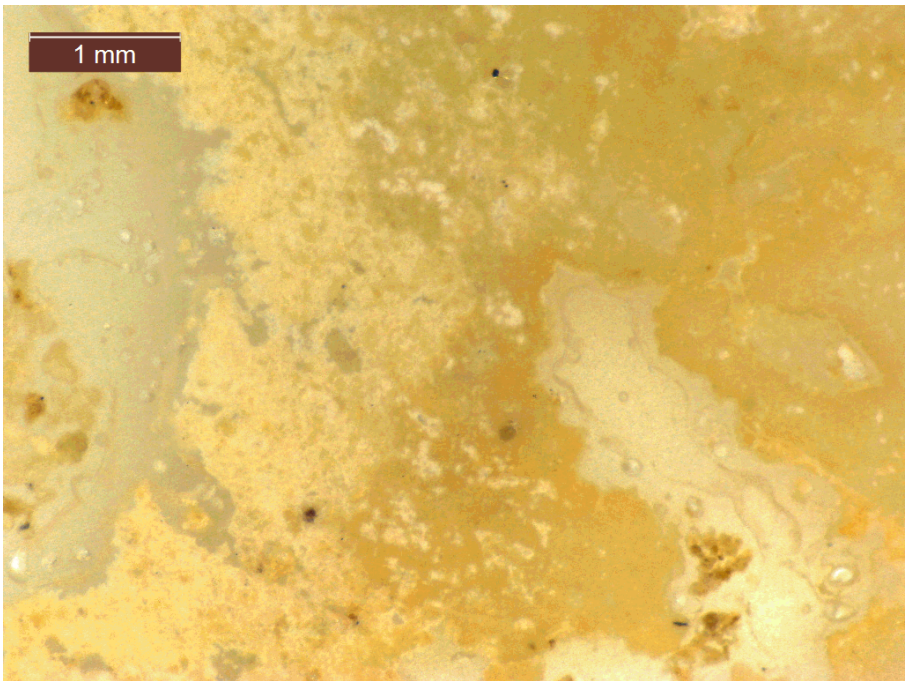

Figure 32. C’’’’, thin section before stain

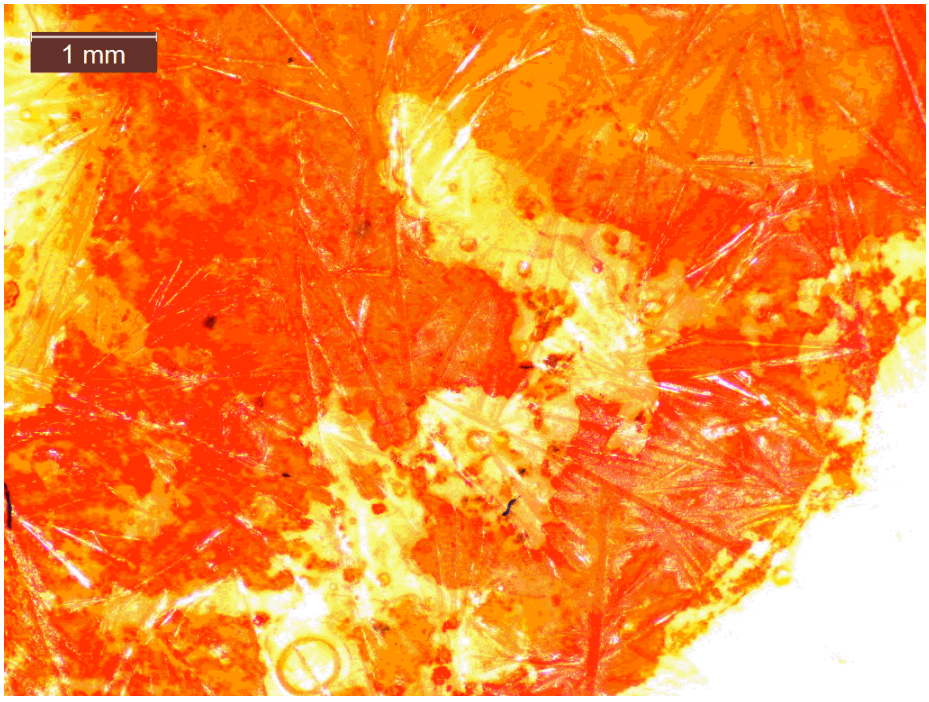

Figure 33. sC’’’, thin section after stain, high Mg carbonate formed along the margin in the top right corner

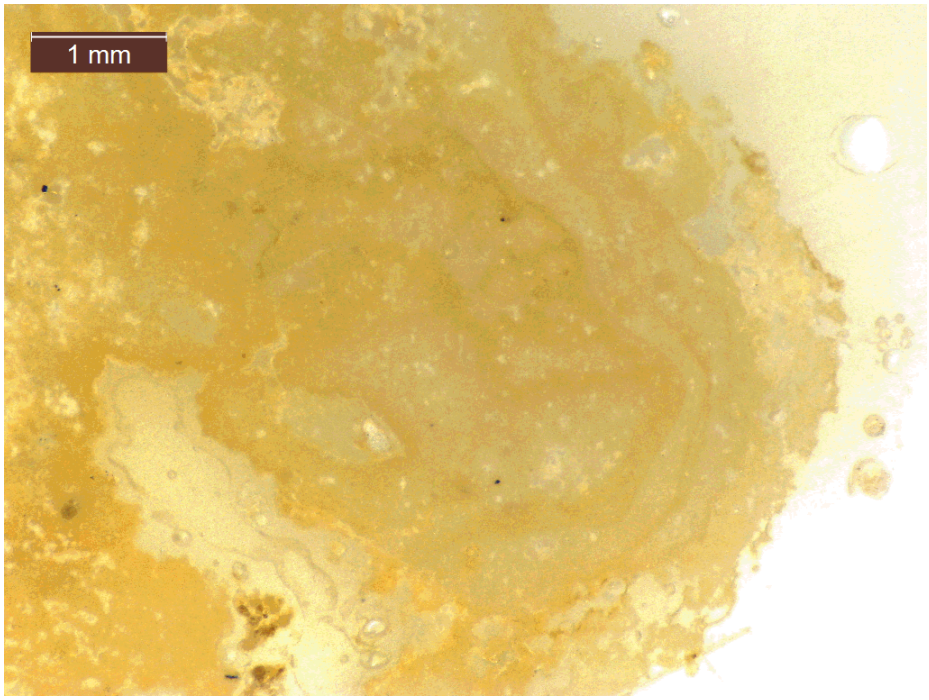

Figure 34. D, thin section before stain, parallel laminae was captured

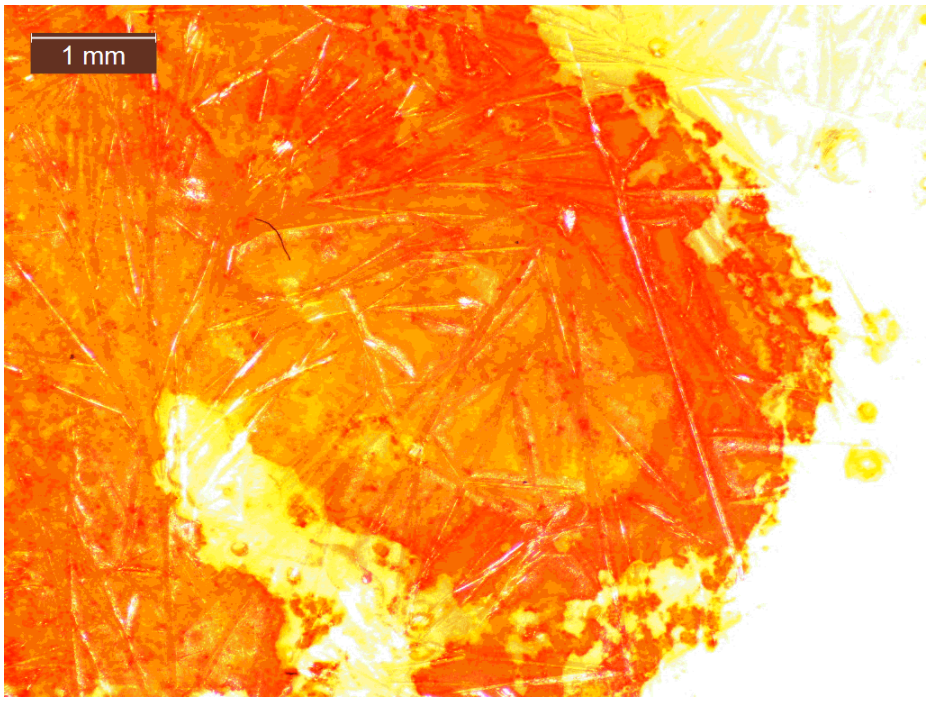

Figure 35. sD, thin section after stain, high Mg carbonate formed along the margin

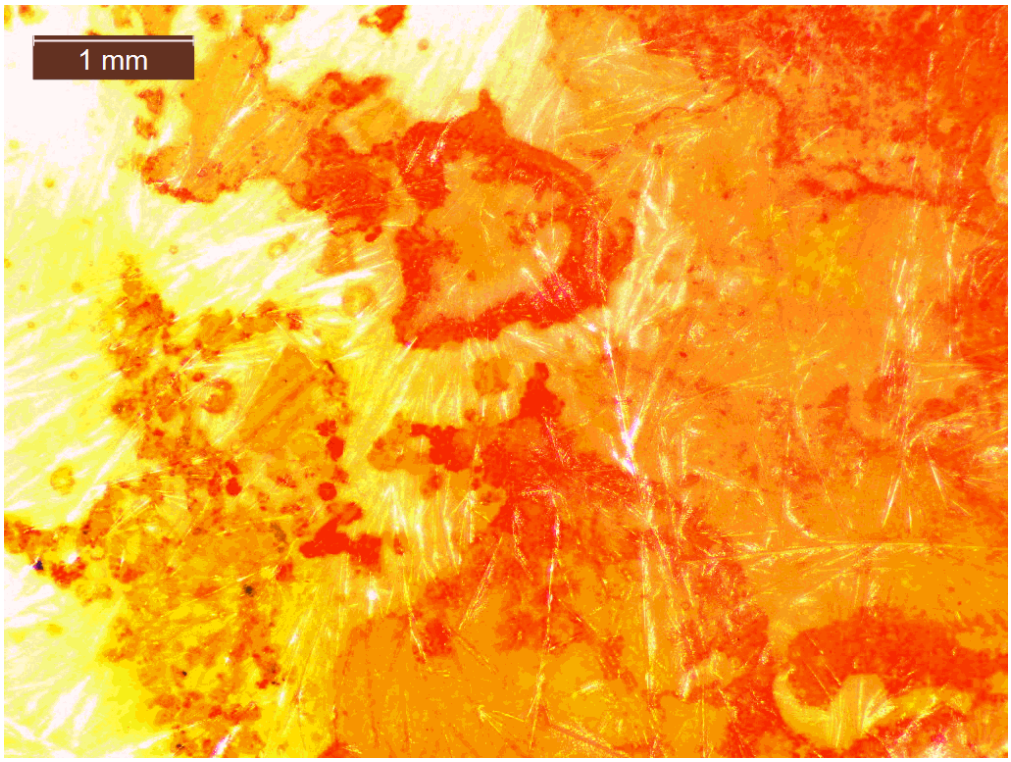

Figure 36. s1, low Mg carbonate spherules that are 1 mm in diameter surrounded by high Mg carbonate

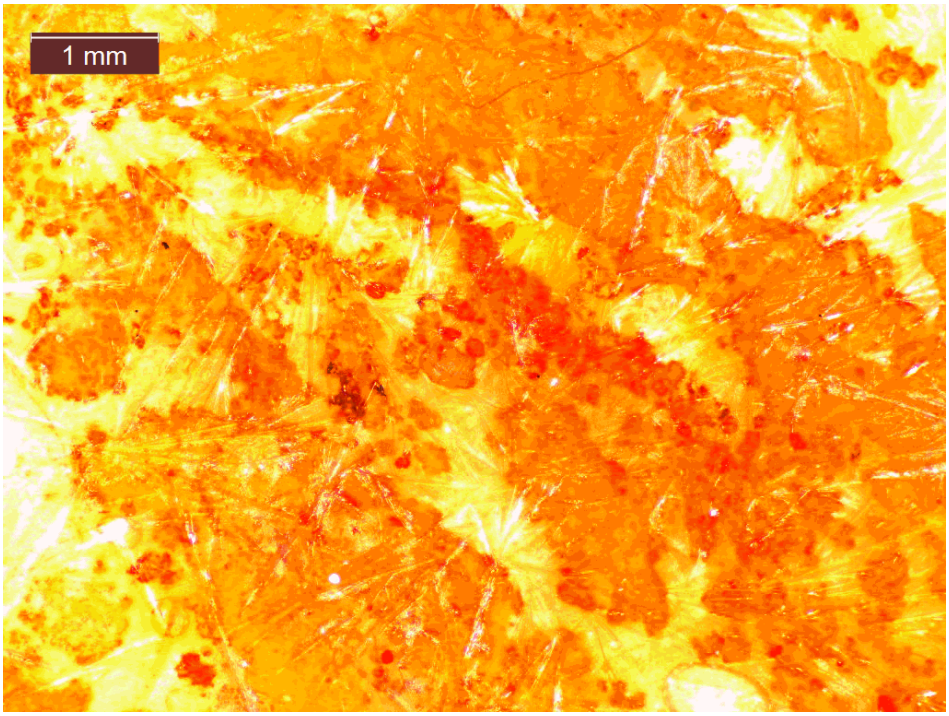

Figure 37. s2, low Mg carbonate with relatively smaller size

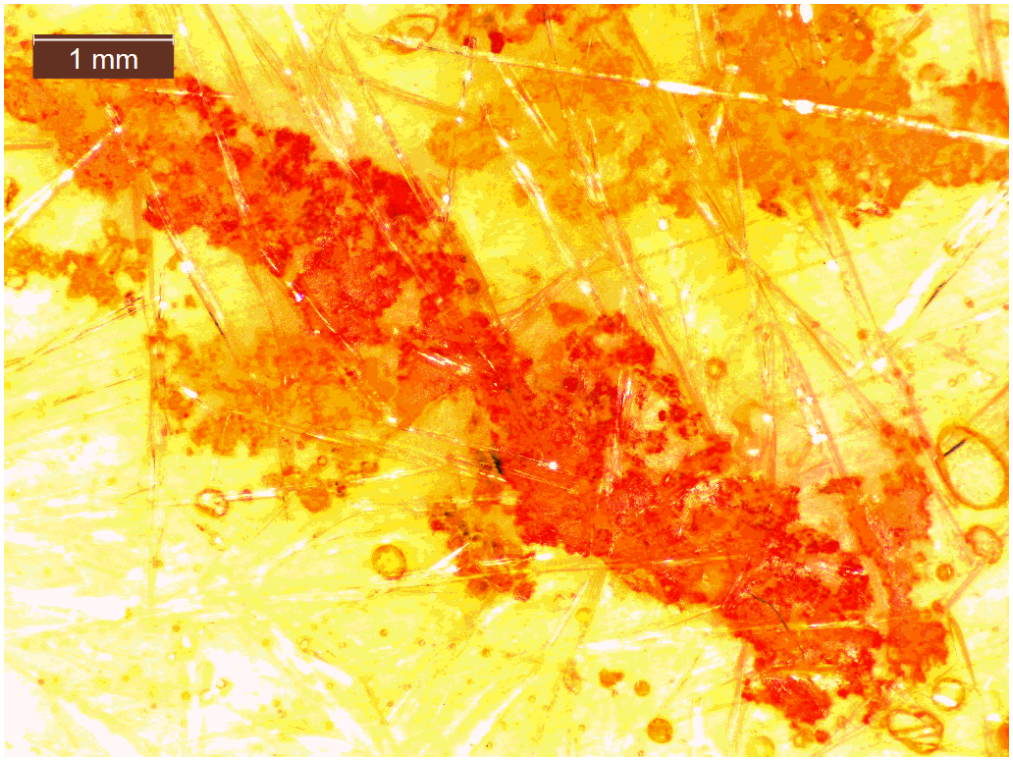

Figure 38. s3, high Mg carbonate formed rod-like

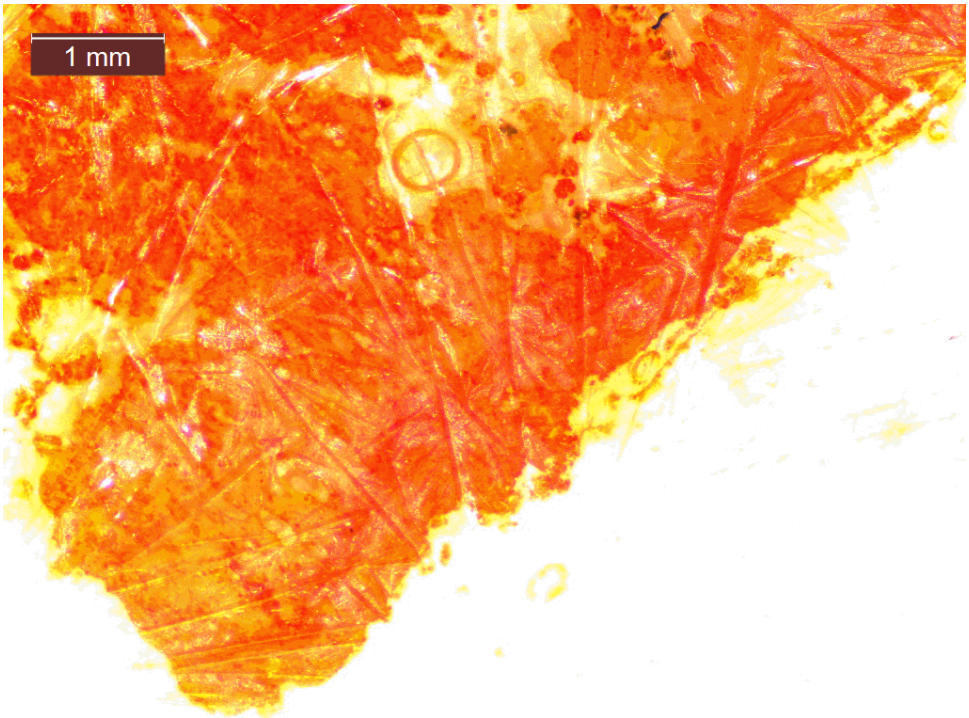

Figure 39. s4, thin section after stain

SEM Results

With the Scanning Electron Microscope (SEM), 5 backscattered electron images, 5 Energy Dispersive X-ray Analyzer (EDX) spot analysis images and 3 elemental mapping images were captured. Each EDX analysis image corresponds to a spot on backscattered electron image. Elemental mapping images show the spatial distribution of 3 different elements (Ca, Sr, Mg), indicating that brighter the chemical zonation the higher the concentration.

Figure 40 represents shows boundary area of two substances. One is locateds at in the left side section with dark, solid materials. The other is locateds at in the right side section containing crystalline structure with light color. A preliminary deduction is: left section is organic matter or epoxies, while right section is one of two major minerals (high-Mg calcite & or aragonite) existing in stromatolites. Based on EDX analysis of left side section (Figure 41), there are quantities of carbon and small amount of magnesium, indicating those dark, solid materials are carbon-rich and highly likely organic matter. Moreover, an EDX analysis of epoxies (Figure 42) reveals the appearance of iron and copper, which is further evidence that excludes the possibility of those dark, solid materials being high-Mg calcite or aragonite and supports the preliminary conjecture.

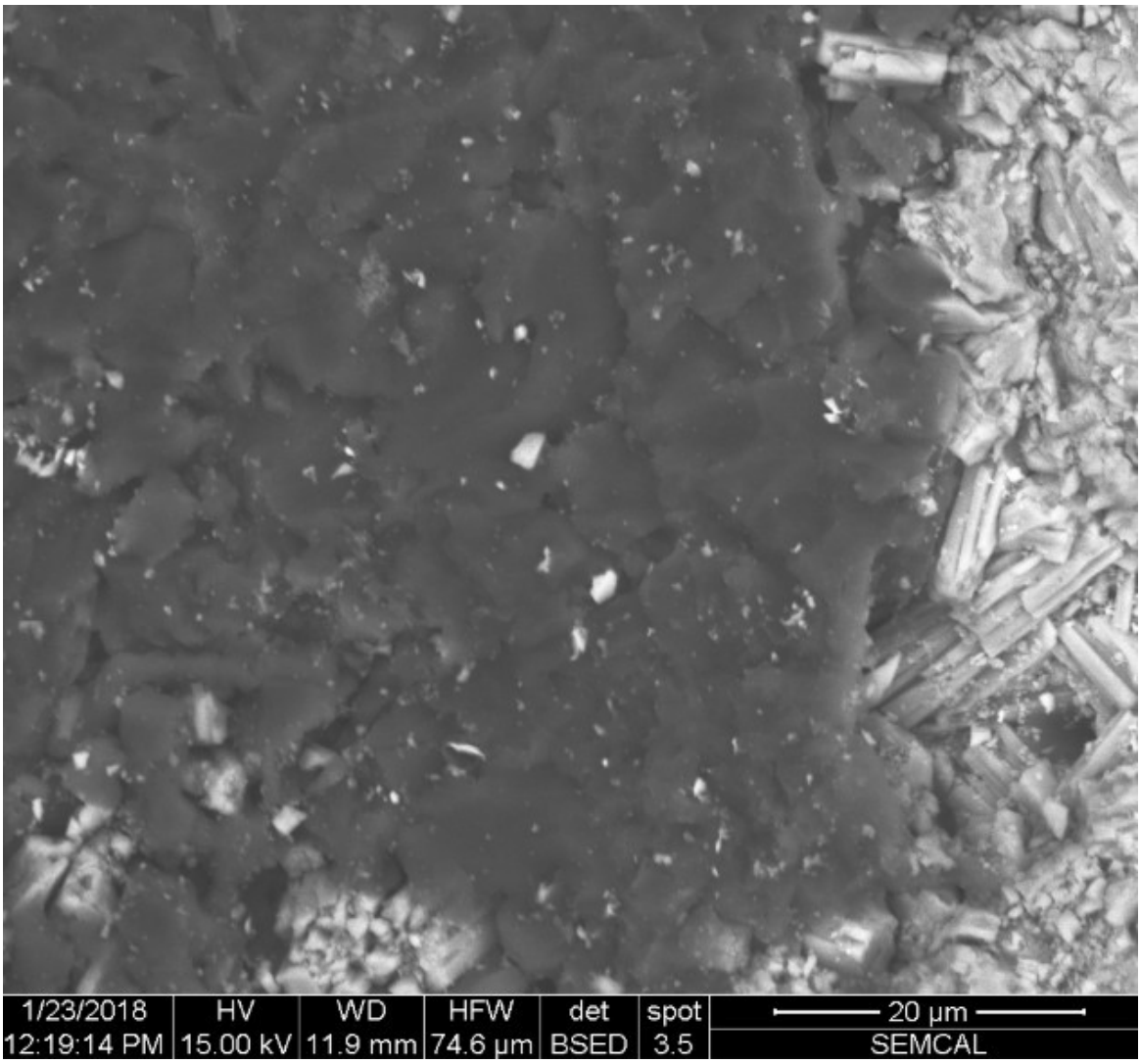

Figure 40. Backscattered electron image of boundary area of organic matter (left side, dark materials) and aragonite lath (right side, light color)

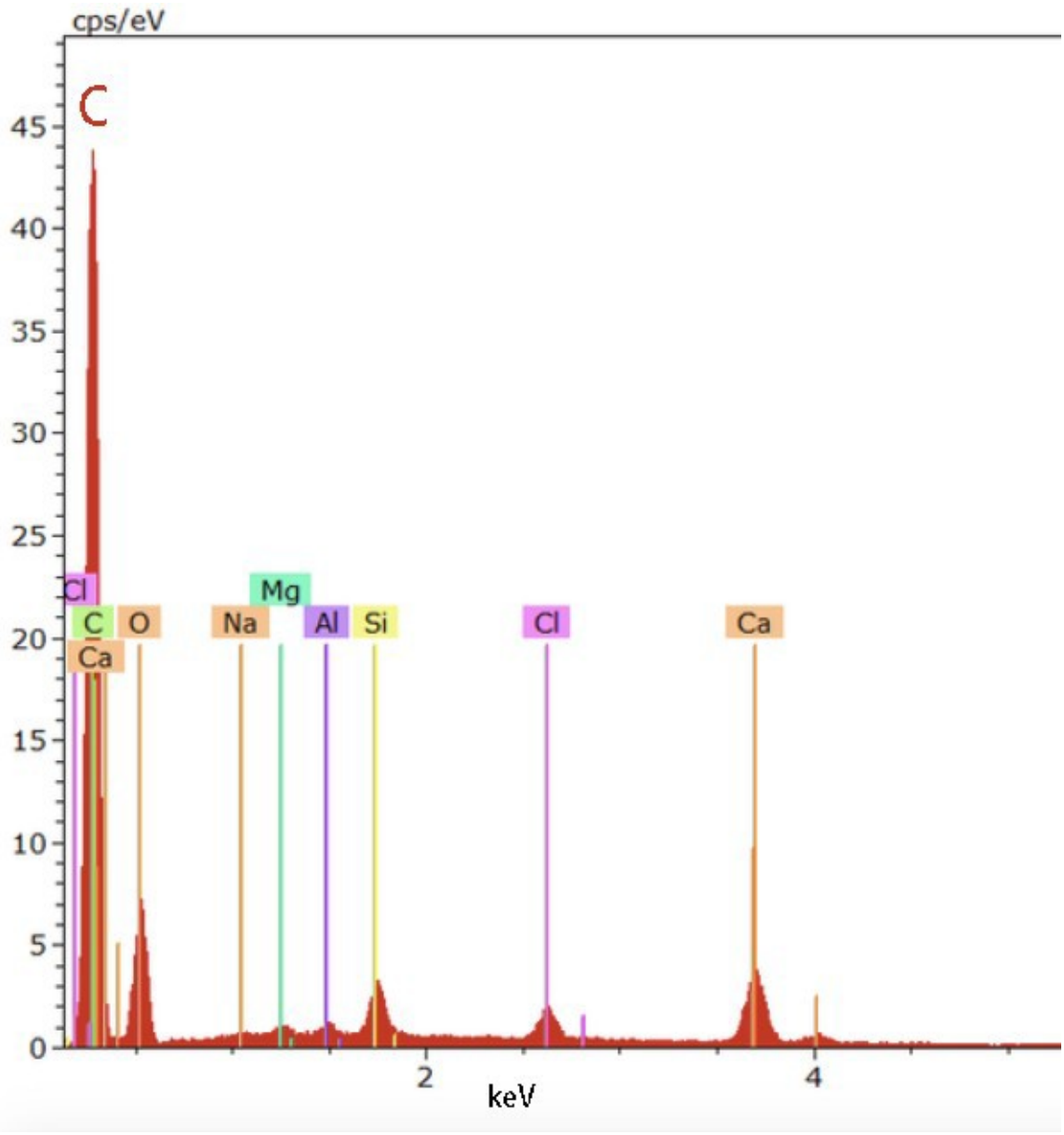

Figure 41. EDX analysis of left side materials, showing a large peak of carbon, and small peak of magnesium

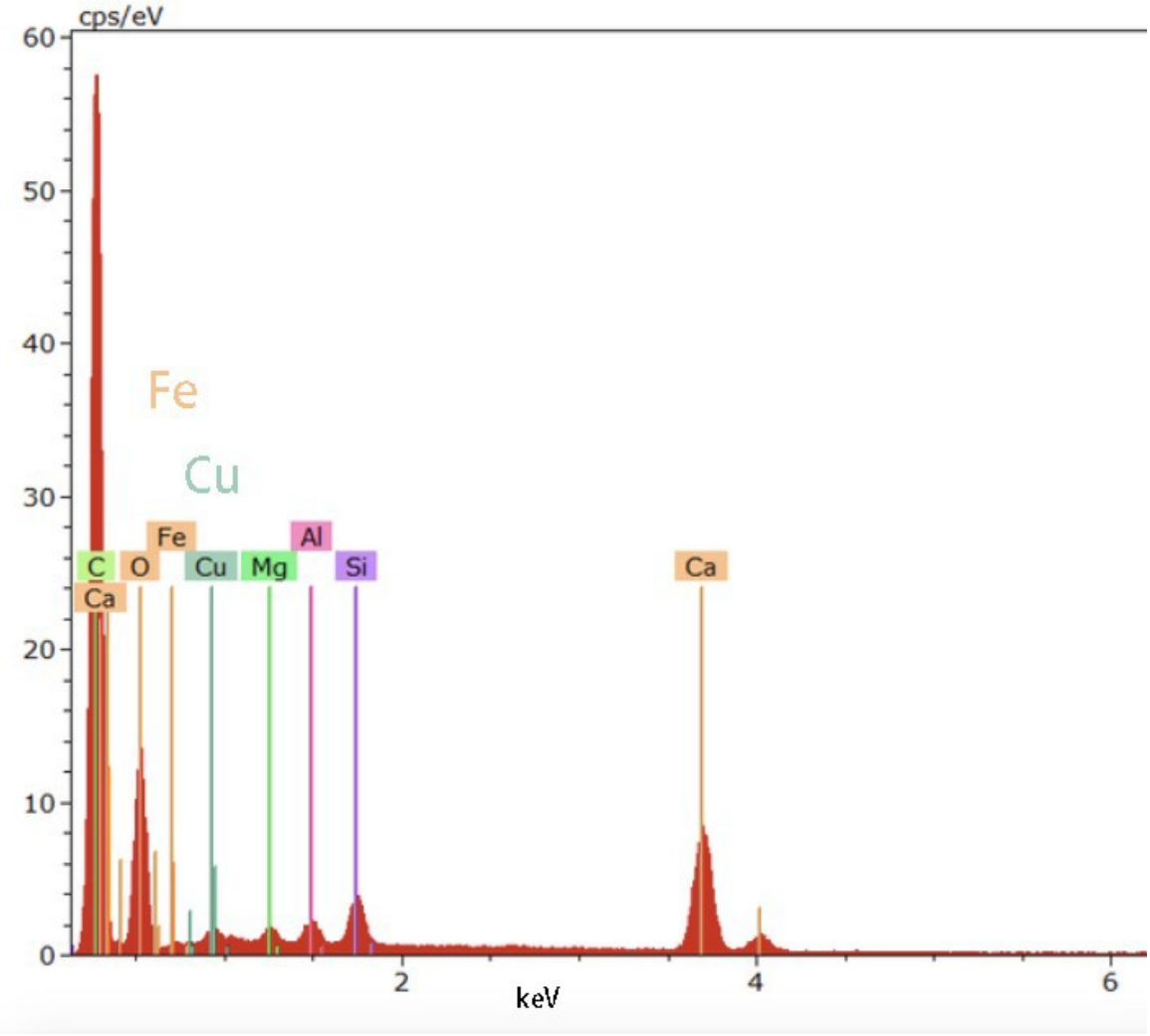

Figure 42. EDX analysis of epoxies, slight amount of iron and copper were detected

Figure 43 shows the mineral located on the right side of Figure 40, which is probably high-Mg calcite or aragonite. Image shows an aggregate of fibrous crystals, crystal morphology is lath-like. EDX analysis of the mineral (Figure 44) reveals a peak of strontium and relatively small amount of magnesium, indicating the mineral is aragonite.

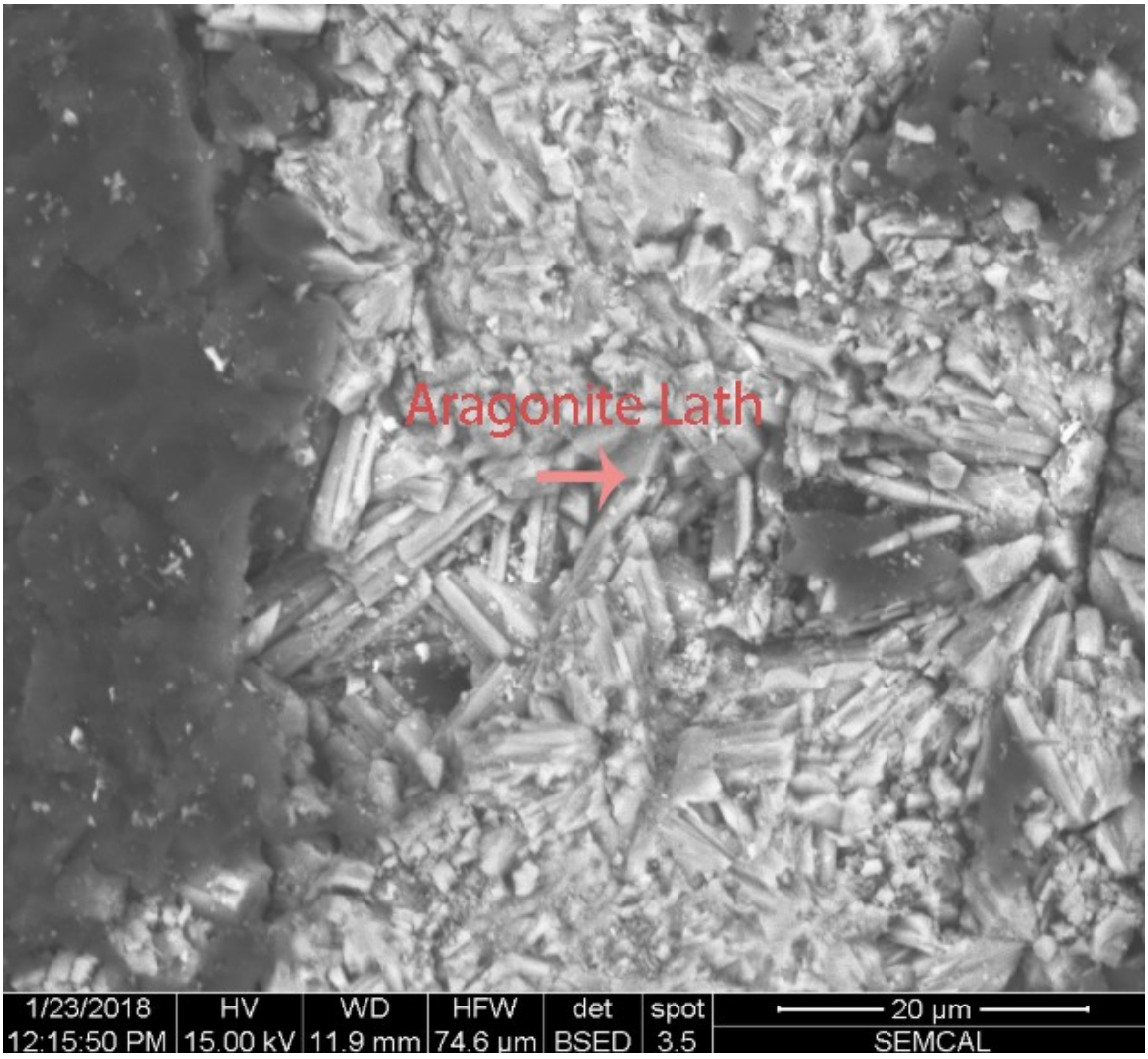

Figure 43. An aggregate of fibrous aragonite crystals with lath-like morphology

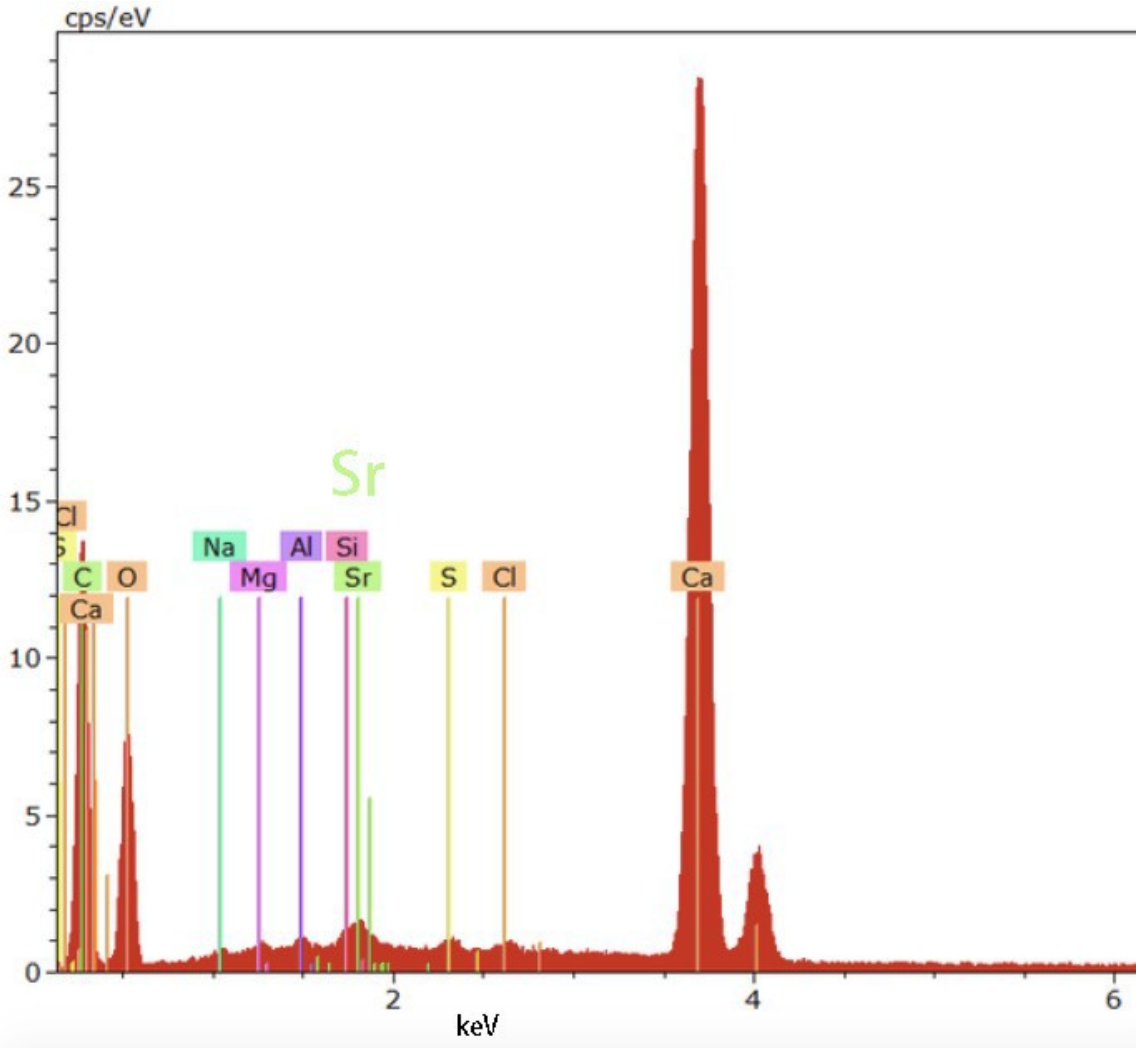

Figure 44. EDX analysis of aragonite, showing a peak of Sr and a smaller peak of Mg

Viewed with smaller magnification, there is a large area of light color minerals (Figure 45), assuming it aragonite. For further information, EDX analysis (Figure 46) was used on a spot of the light color minerals, displaying elemental abundances similar to Figure 44. For instance, there is a peak of Sr and a relatively a smaller peak of Mg. This exercise indicates that within a smaller magnification, aragonite represents a light color.

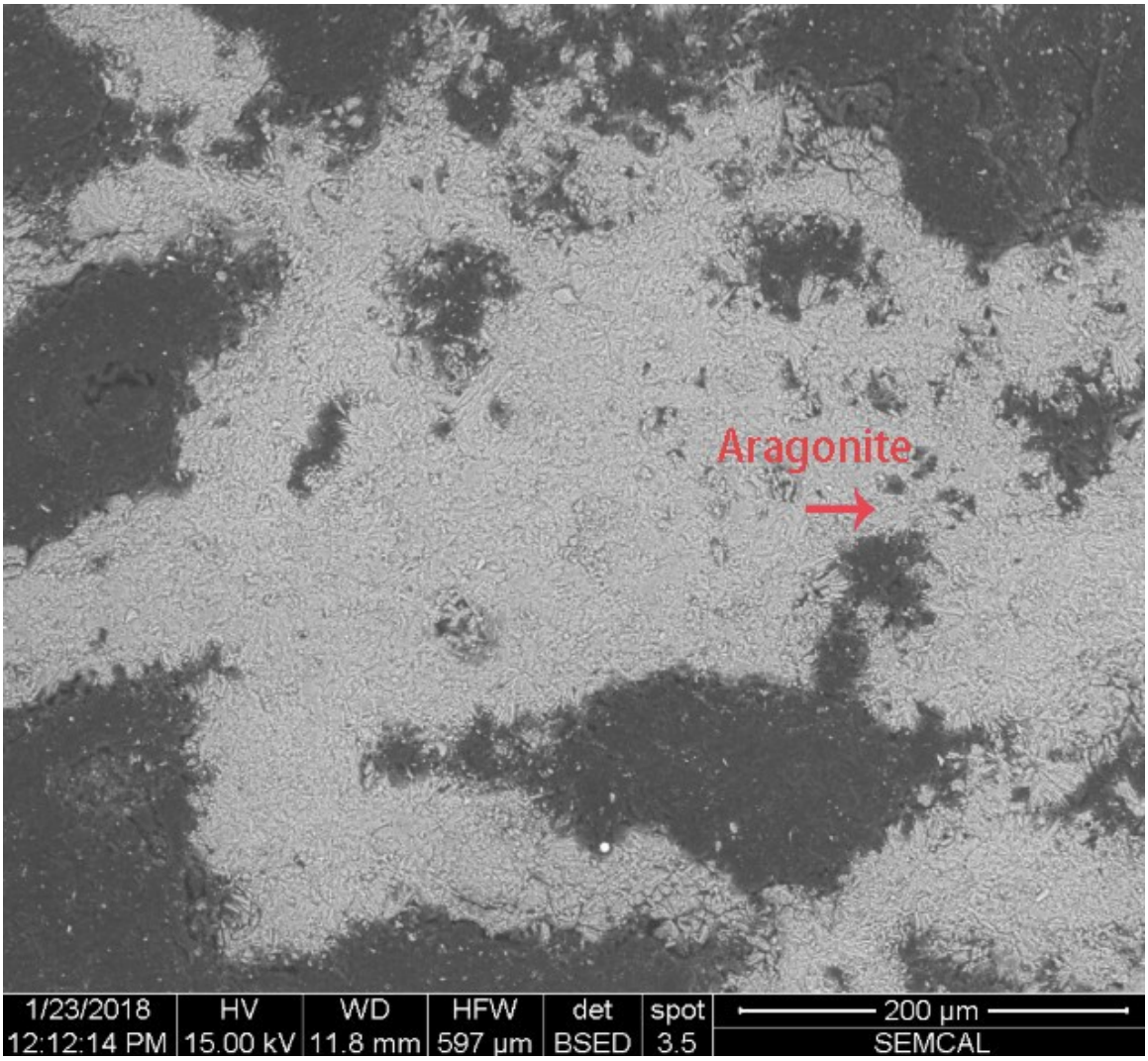

Figure 45. Backscattered electron image of aragonite (light color) at low magnification (x350)

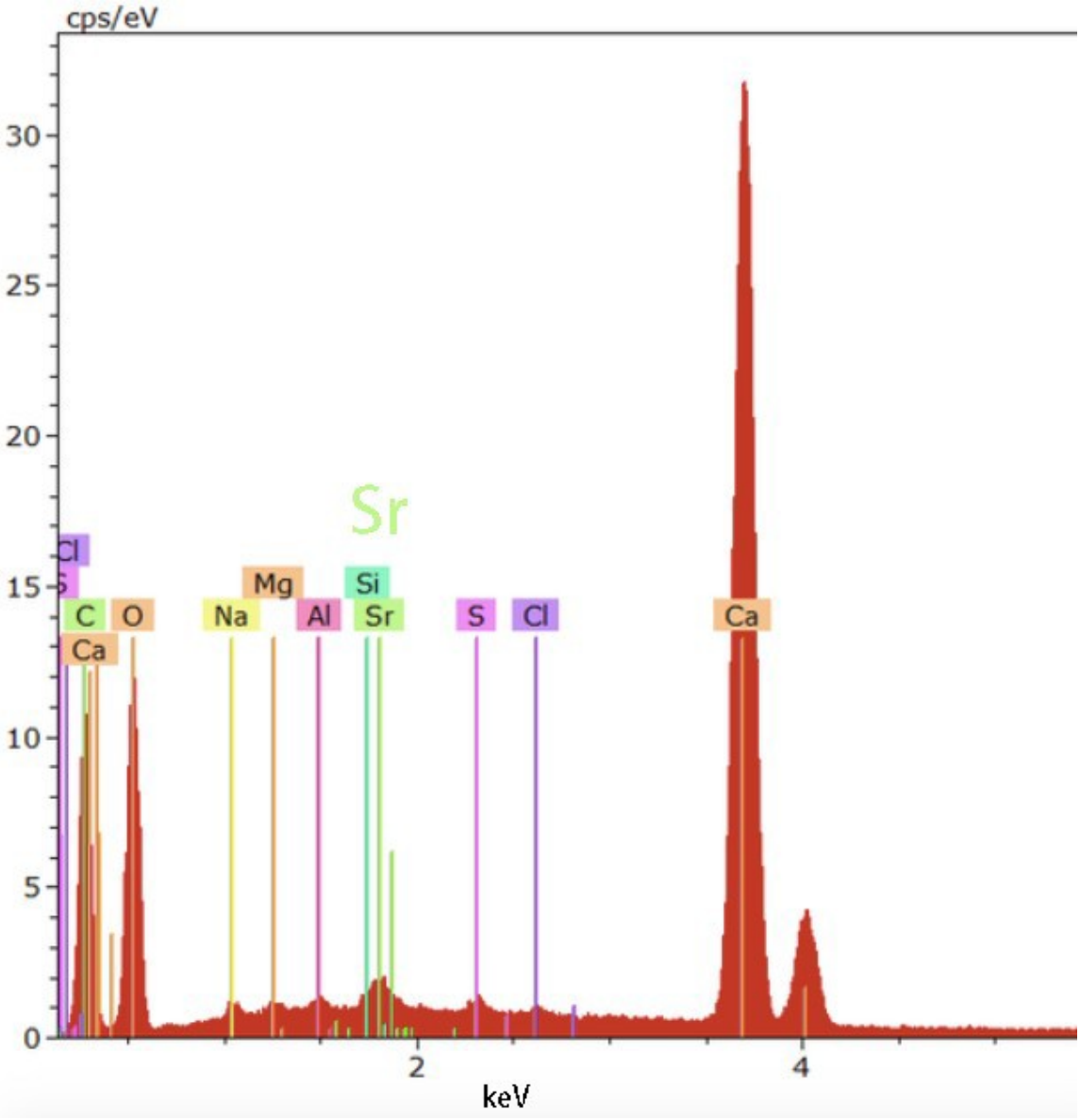

Figure 46. EDX analysis of light color mineral (aragonite) reveals a peak of Sr and a relatively lesser amount of Mg, similar to elemental abundances in Figure 44

In Figure 47, distribution of two materials of different colors was represented. One is with lighter color, authenticating it is aragonite. The other material is with darker color, speculating it is high-Mg calcite. EDX analysis (Figure 48) also supports the hypothesis, showing a peak of relatively larger amount of Mg.

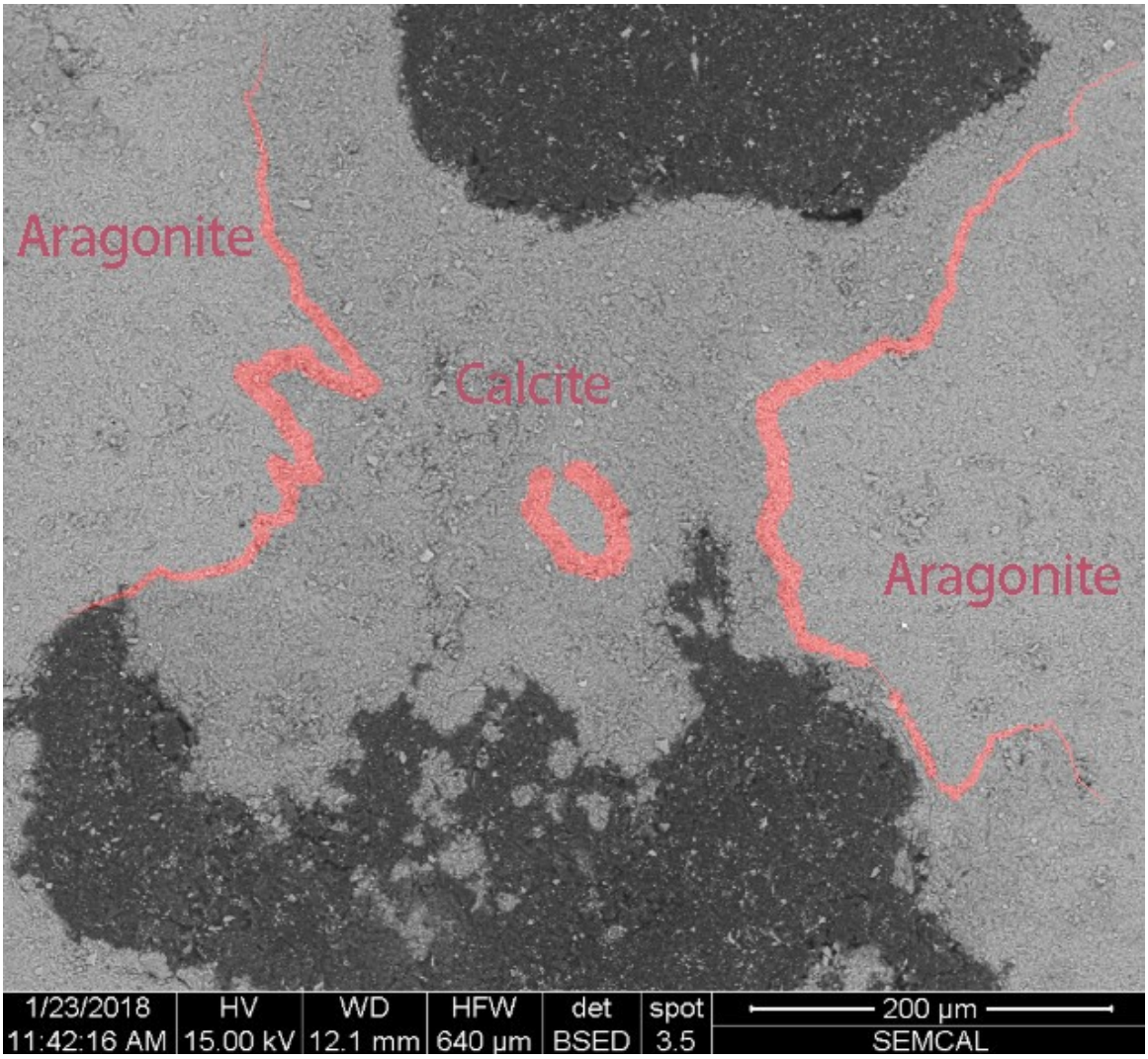

Figure 47. Distribution of lighter and darker minerals, which are aragonite and high-Mg calcite respectively

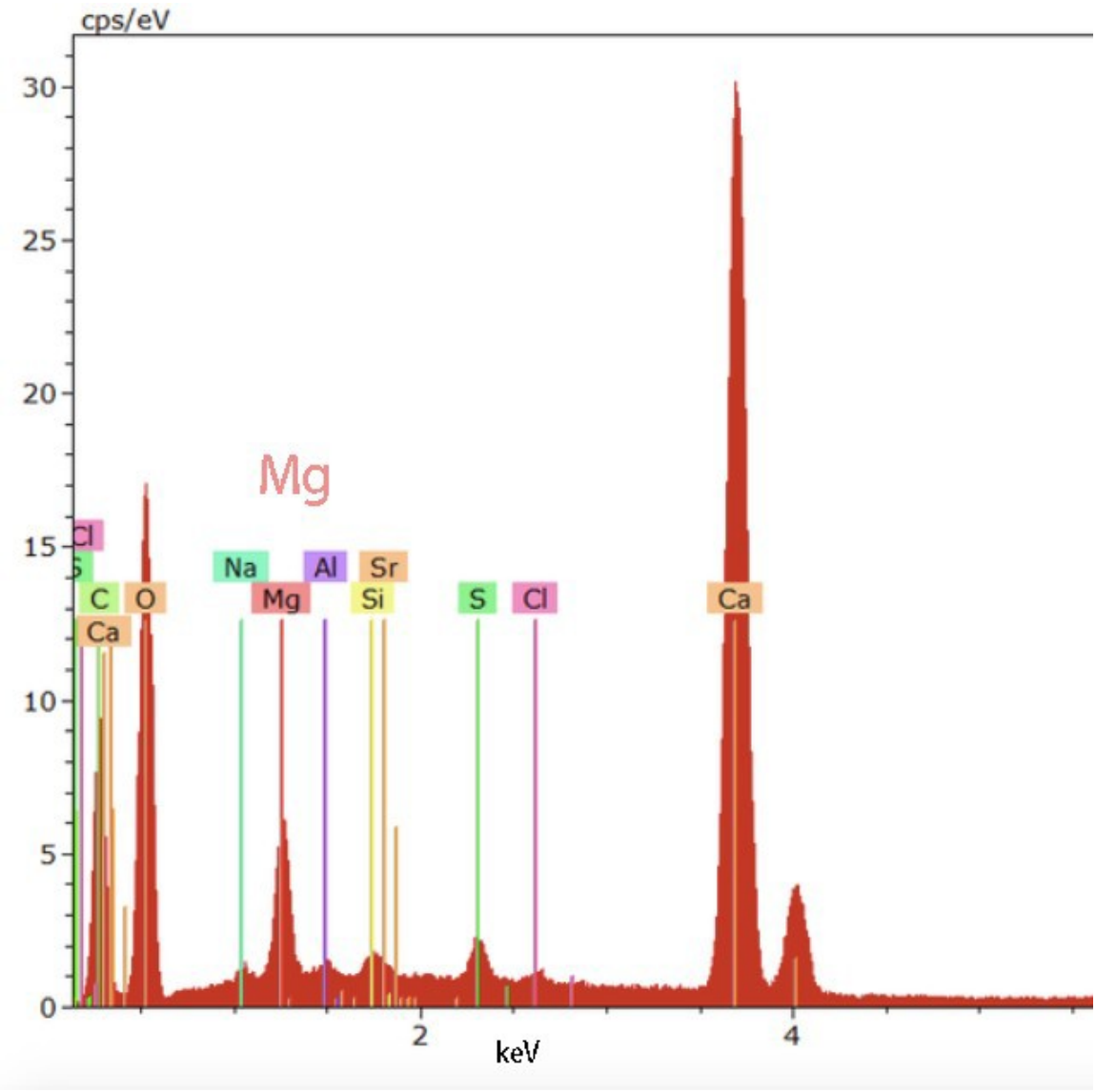

Figure 48. EDX analysis of darker color mineral reveals there is a relatively larger amount of Mg, indicating it is high-Mg calcite

Elemental maps based on Ca (Figure 50), Mg (Figure 51) and Sr (Figure 52) of Figure 49 (right side of Figure 47), show the arrangement of high-Mg calcite and aragonite. According to elemental mapping methods, the brighter the chemical zonation, and the higher the concentration. In Figure 50, the lighter area is Ca-rich, indicating the area is high-Mg calcite and aragonite. For Figure 51 and 52, the spatial distributions of Mg and Sr correspond to each high Mg calcite and aragonite, respectively. Mg-rich areas in figure 51 becomes Sr-poor in figure 52 and vice versa, which further affirms the distribution based on color difference.

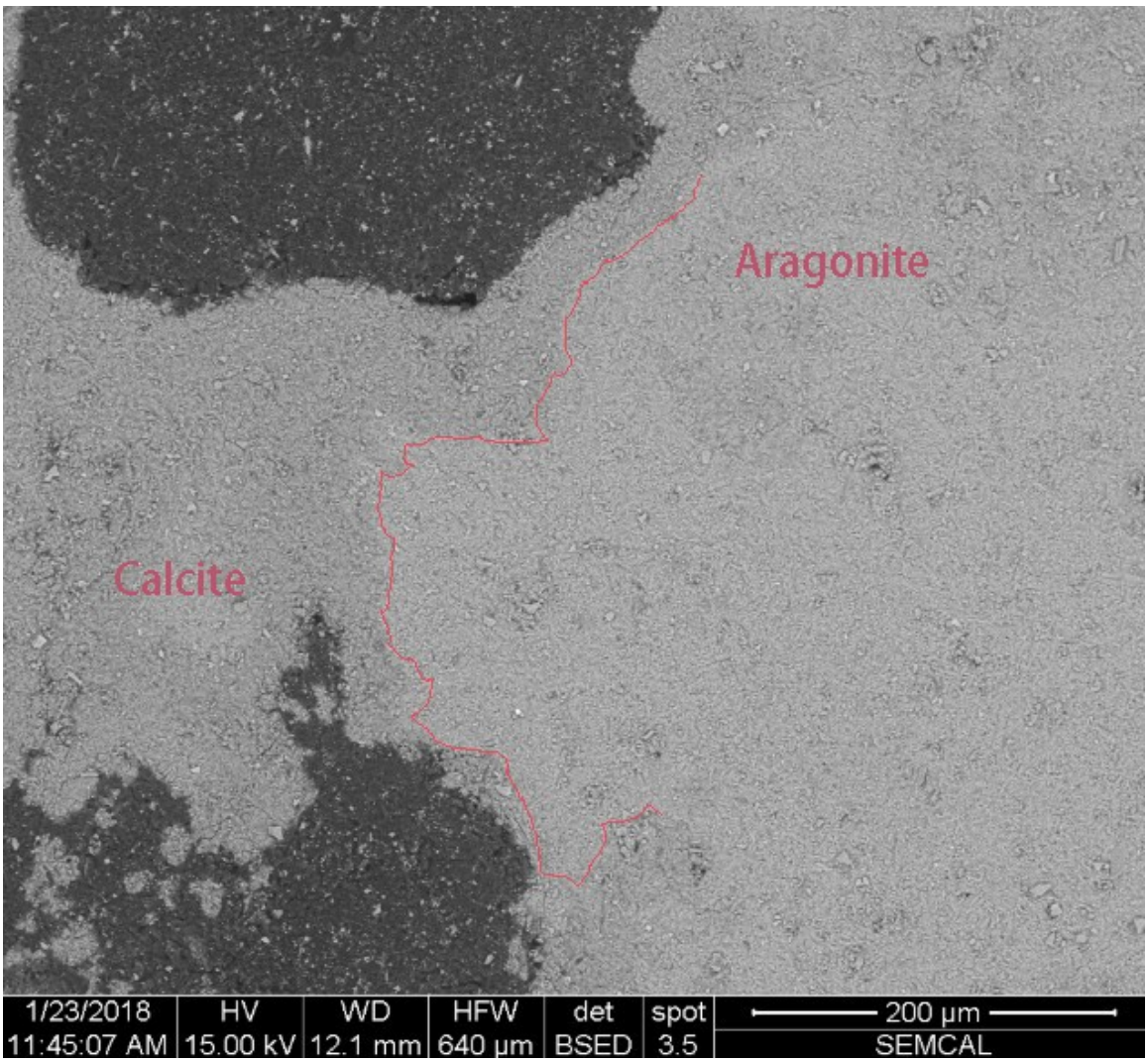

Figure 49. Backscattered electron image of designated area, located on the right side of Figure 47, based on their color difference, spatial arrangement was roughly delineated

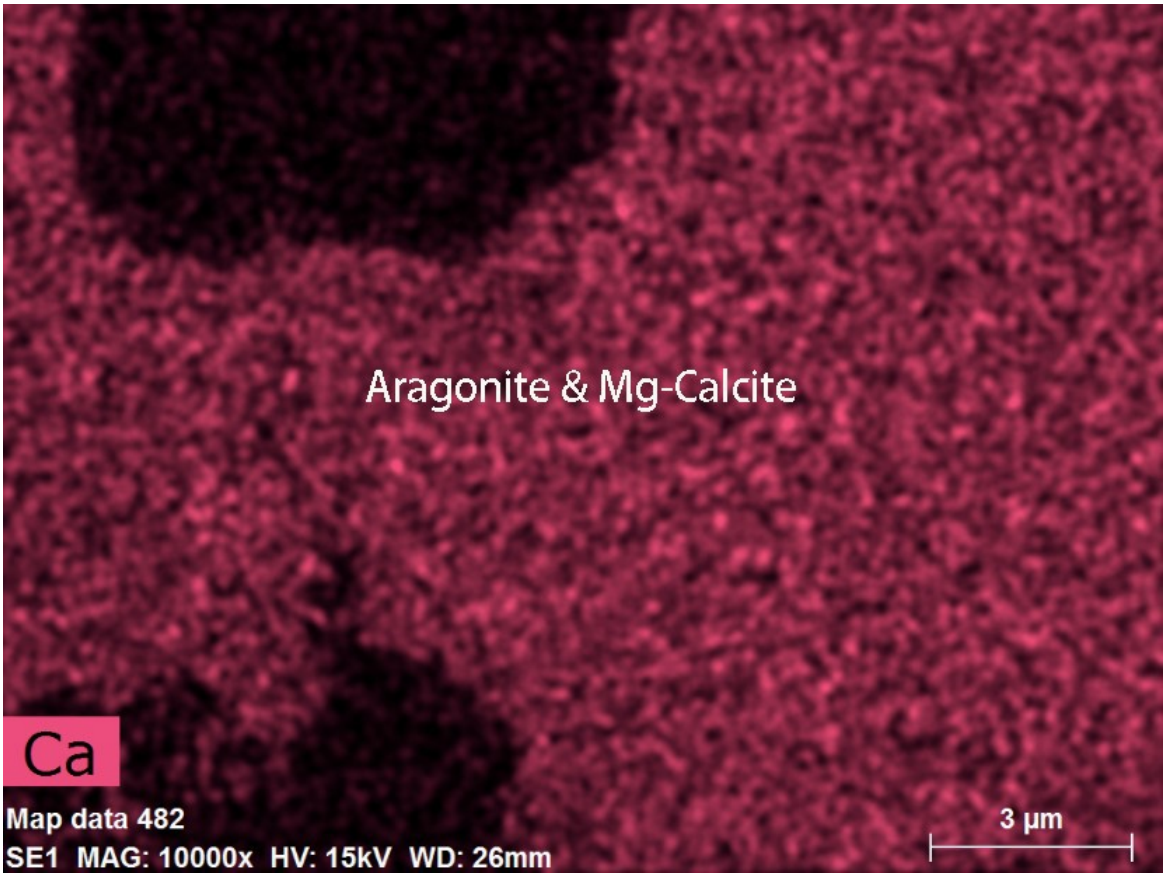

Figure 50. Elemental map of Ca, showing the light pink area is Ca-rich

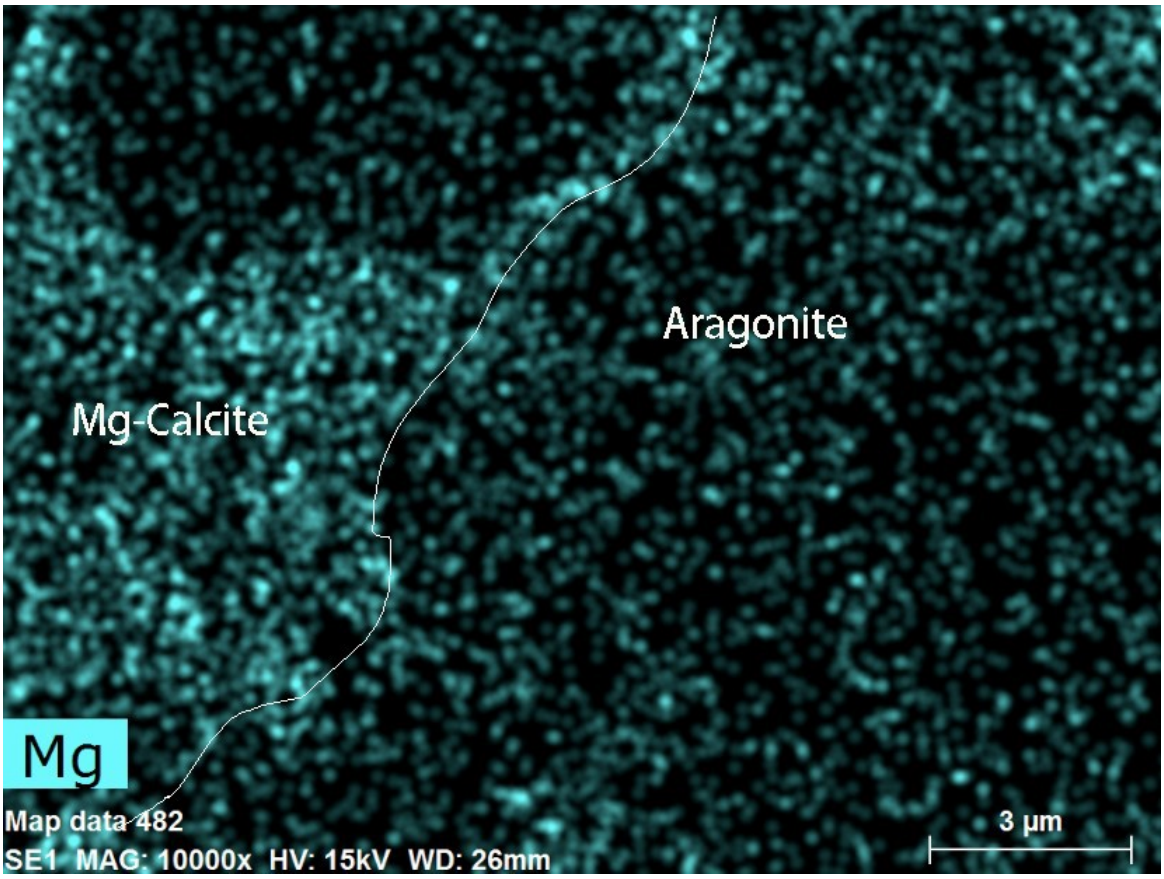

Figure 51. Elemental map of Mg, showing the light blue area is Mg-rich

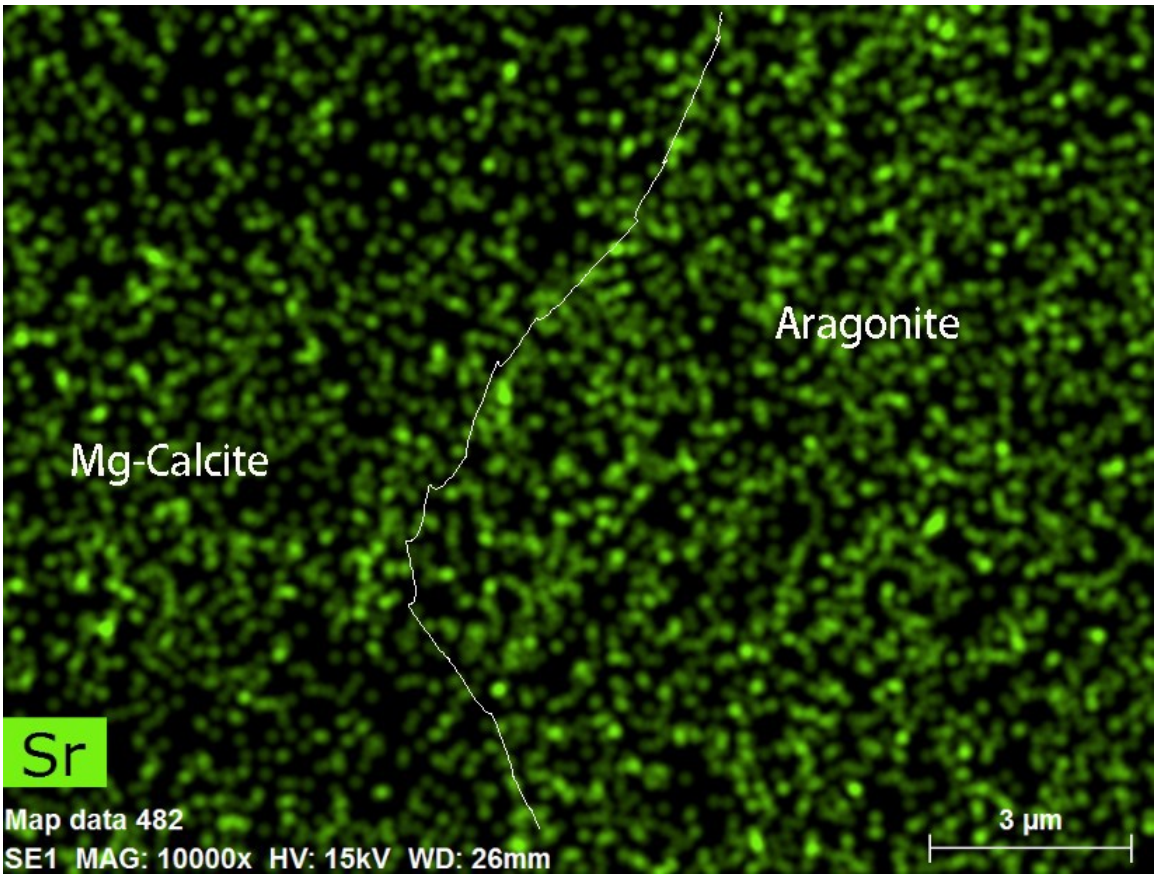

Figure 52. Elemental map of Sr, showing the relatively lighter area is Sr-rich

Discussion

As shown in Figures 9, 13 and 35, light orange interiors representing low-Mg carbonate minerals are surrounded by dark orange exteriors representing high-Mg minerals. According to Choquette and Trusell (1978), aragonite shows a light orange color; high-Mg calcite shows a dark orange color in the stained sample investigated. Moreover, as depicted in Figure 36, an aragonite spherule is surround by high-Mg calcite.

It is commonly assumed that interiors of the stromatolitic knobs represent older growth and therefore, aragonite formed first and Mg-calcite formed later. Moreover, calcite is more stable in general than aragonite and it has been shown that aragonite can spontaneously turn into calcite over geologic time (Boulos et al., 2014).

However, more recently, experimental studies of Konrad et al. (2018) found that amorphous calcium carbonate stability and its phase development are controlled to a large extent by aqueous Mg concentration in the reaction solution. With higher Mg^{2+} concentration ($>$0.055 M Mg^{2+}) in solution, aragonite was formed as the final reaction product. Han et al. (2018) also indicated that Mg^{2+} ions in solution could induce the precipitation of calcium carbonate to form aragonite crystals and inhibit the process of polymorphic transformation from aragonite to calcite. According to Li (2017), the Mg^{2+} concentration of this study site is 0.06 M on average, which corresponds to the precondition of aragonite formation in the study by Konrad et al. (2018). Further, as a final reaction product, Konrad et al. (2018) also indicated for the aggregation of aragonite, it was found to form ~200-300 nm crystals aggregating into ~2 μm sized rods.

As shown in an SEM image (Figure 43), 10 μm sized aragonite laths and 500 nm aragonite fragments both exist, indicating that calcium carbonate phase transformation was not accomplished completely by the time the sample was collected. Thus, the possibility that aragonite was formed as a final product cannot be ruled out considering the high magnesium concentration in Storr's Lake.

Conclusion

To determine the spatial arrangement and distribution of aragonite and Mg-calcite in stromatolite from our study site, and hence to deduce the sequential order of minerals' formation, Titan-Yellow staining and Scanning Electron Microscopy were adopted.

Several microscopic components make up the stromatolites. These components include: high-Mg calcite, aragonite, and organic matter. After Titan-Yellow staining, Mg-calcite showed the color of dark orange while aragonite showed the color of light orange in a prepared thin section. The stromatolitic intervals include oriented, wavy to parallel carbonate and organic-rich laminae. Some peculiar features observed, including wavy Mg-calcite laminae parallel to margins, as well as, rare aragonite spherules that are 1 mm in diameter surrounded by Mg-calcite. Moreover, botryoidal aragonite is either discontinuous (distinct botryoids) or forms more continuous laminae (coalesced botryoids). A SEM image showed an aggregate of fibrous crystals, which is aragonite, crystal morphology is lath-like. In this image, 10 μm sized aragonite laths and 500 nm aragonite fragments both exist.

The overall trend of aragonite and Mg-calcite distribution in the investigated stromatolite section is aragonite growing internally while Mg-calcite growing externally. Ultimately, these stromatolites are of late Holocene age and grow with growth rate approxiamtely 16 cm per 1000 years (Paull et al., 1992) in broadly analogous conditions: low energy setting, highly alkaline and saline lake. Even though interiors of the stromatolitic knobs represent older growth and aragonite is less stable than calcite, the formation process of these two minerals in stromatolites is still indistinct because the high Mg concentration in reactive solution plays a vital role in deciding the formation order according to recent researches.

Suggestions for Future Research

A lot more work needs to be completed to determine why high-Mg calcite is forming along margins and covering aragonite with uneven size crystals existing at same time. Also, the sequential order of formation process is still unsolved problem regarding for the high Mg concentration in Storr's Lake. However, the data related to it were collected from experiments so far, whether the result is transferable to study site in nature environments still needs to be discussed.

REFERENCES

Allwood, A.C., Walter, M.R., Burch, I.W., Kamber, B.S., 2007, 3.43 billion-year-old stromatolite reef from the Pilbara Craton of Western Australia: Ecosystem-scale insights to early life on Earth: Precambrian Research, v. 158, p. 198–227, doi: 10.1016/j.precamres.2007.04.013.

Allwood, A.C., Walter, M.R., Kamber, B.S., Marshall, C.P., Burch, I.W., 2006, Stromatolite reef from the Early Archaean era of Australia: Nature, v. 441, p. 714- 718, doi: 10.1038/nature04764.

Bosak, T., Knoll, A.H., Petroff, A.P., 2013, The Meaning of Stromatolites: Annual Review of Earth and Planetary Science, v. 41, p. 21-44, doi: 10.1146/annurev-earth-042711-105327.

Boulos, R.A., Zhang, F., Tjandra, E.S., Martin, A.D., Spagnoli D., 2014, Spinning up the polymorphs of calcium carbonate: Scientific Reports, 4:3616, doi: 10.1038/srep03616.

Burne, Robert V., Moore, Linda S., 1987, Microbialites: organosedimentary deposits of benthic microbial communities: Palaios, v. 2, p. 241-254, doi: 10.2307/3514674.

Choquette, P.W., Trusell, F. C., 1978, Procedure for Making Titan-yellow Stain for Mg-Calcite Permanent: Journal of Sedimentary Petrology, v. 48, p. 639-641, doi: 10.1306/212F74FF-2B24-11D7-8648000102C1865D.

Curran, H.A., 1997, Introduction to the Geology of the Bahamas and San Salvador Island, with an Overflight Guide, In Curran, H.A., (ed.), Guide to Bahamian Ichnology: Pleistocene, Holocene, and Modern Environment, Bahamian Field Station, San Salvador, Bahamas.

Dupraz, C., Strasser, A., 1999, Microbialites and micro-encrusters in shallow coral bioherms (Middle-Late Oxfordian, Swiss Jura Mountains): Facies, v. 40, p. 101-130, doi: 10.1007/BF02537471.

Fowler, A.J., 2011, Stromatolitic Knobs in Storrs Lake, San Salvador, Bahamas: Insights into Organomineralization [M.S. thesis]: University of Connecticut, 180 p.

Glumac, B., Savarese, M., 2016, Geology of the Bahamas and Other Carbonate Regions, *in* Proceedings, Symposium, 16th: San Salvador, Bahamas, Gerace Research Center. Han, Y., Zhang, C., Wu, L., Zhang, Q., Zhu, L., Zhao, R., 2018, Influence of alternating electromagnetic field and ultrasonic on calcium carbonate crystallization in the presence of magnesium ions: Journal of Crystal Growth, v. 499, p. 67-76, doi: 10.1016/j.jcrysgro.2018.07.037

Hattin, D.E., 1982, Geology of the Bahamas, *in* Proceedings, Symposium, 1st:San Salvador, Bahamas, College Center of the Finger Lake.

Hofmann, H.J., Grey, A.H., Hickman, A.H., Thorpe, R.I., 1999, Origin of 3.45Ga coniform stromatolites in Warrawoona Group, Western Australia: Geological Society of America Bulletin, v. 111, p. 1256-1262, doi: 10.1130/0016-7606(1999)111<1256:OOGCSI>2.3.CO;2.

Konrad, F., Purgstaller, B., Gallien, F., Mavromatis, V., Gane, P., Dietzel, M., 2018, Influence of aqueous Mg concentration on the transformation of amorphous calcium carbonate: Journal of Crystal Growth, v. 498, p. 381-390, doi: 10.1016/j.jcrysgro.2018.07.018.

Li, Z., 2017, Magnesium Isotope Investigation of Stromatolitic Knobs in Storr's Lake, San Salvador, Bahamas: Implications for Organomineralization and Laminae Formation [M.S. thesis]: The University of Texas at Arlington, 201 p.

Mann, C.J., Nelson, W.M., 1989, Microbialitic structures in Storr's Lake, San Salvador Island, Bahamas Islands: Palaios, v. 4, p. 287-293, doi: 10.2307/3514777.

Monty, C.L.V., 1977, Evolving concepts on the nature and the ecological significance of stromatolites. In Flügel, E., eds., Fossil Algae: Springer, Berlin, Heidelberg, p. 15-35, doi: 10.1007/978-3-642-66516-5_2.

Neumann, C.A., Bebout, B.M., McNeese, L.R., Paul, C.K., Paerl, H.W., 1989, Modern stromatolites and associated mats: San Salvador, Bahamas, *in* Proceedings, Symposium on the Geology of the Bahamas, 4th: Bahamas Field Station, San Salvador, Bahamas, p. 235-251.

Park, L., 2012, Comparing two long-term hurricane frequency and intensity records from San Salvador Island, Bahamas: Journal of Coastal Research, v. 28, p. 891-902, doi: 10.2112/JCOASTRES-D-11-00065.1

Paul, V.G., Wronkiewicz, D.J., Mormile, M.R., 2016, Mineralogy and microbial diversity of the microbialites in the hypersaline Storr's Lake, the Bahamas: Astrobiology, v. 16, p. 282–299, doi: 10.1089/ast.2015.1326.

Paull, C.K., Neumann, A.C., Bebout, B., Zabielski, V., Showers, W., 1992, Growth rate and stable isotopic character of modern stromatolites from San Salvador, Bahamas: Palaeogeography, Palaeoclimatology, Palaeoecology, v. 95, p. 335-344, doi: 10.1016/0031-0182(92)90149-Y.

Reid, R.P, James, N.P., Macintyre, I.G., Dupraz, C., Burne, R.V., 2003, Shark Bay Stromatolites: Microfabrics and reinterpretation of origins: Facies, v. 49, p. 45-53, doi: 10.1007/s10347-003-0036-8.

Riding, R., 2011, Microbialites, stromatolites, and thrombolites. in J. Reitner and V. Thiel, eds., Encyclopedia of Geobiology: Encyclopedia of Earth Science Series, Springer, Heidelberg, p. 635-654, doi: 10.1007/978-1-4020-9212-1.

Riding, R., 2000, Microbial carbonates: the geological record of calcified bacterialalgal mats and biofilms: Sedimentology, v. 47, p. 179-214, doi: 10.1046/j.1365-3091.2000.00003.x.

Swapp, S., 2017, Scanning Electron Microscopy (SEM): https://serc.carleton.edu/research_education/geochemsheets/techniques/SEM.html (accessed September 2018).

Zabielski, V.P., 1991, The depositional history of Storr's Lake San Salvador Island, Bahamas [Ph.D. thesis]: University of North Carolina Chapel Hill, 107 p.